creative commons
COMMONS DEED

저작자표시-비영리-변경금지 2.0 대한민국

이용자는 아래의 조건을 따르는 경우에 한하여 자유롭게

- 이 저작물을 복제, 배포, 전송, 전시, 공연 및 방송할 수 있습니다.

다음과 같은 조건을 따라야 합니다:

저작자표시. 귀하는 원저작자를 표시하여야 합니다.

비영리. 귀하는 이 저작물을 영리 목적으로 이용할 수 없습니다.

변경금지. 귀하는 이 저작물을 개작, 변형 또는 가공할 수 없습니다.

- 귀하는, 이 저작물의 재이용이나 배포의 경우, 이 저작물에 적용된 이용허락조건을 명확하게 나타내어야 합니다.
- 저작권자로부터 별도의 허가를 받으면 이러한 조건들은 적용되지 않습니다.

저작권법에 따른 이용자의 권리는 위의 내용에 의하여 영향을 받지 않습니다.

이것은 이용허락규약(Legal Code)을 이해하기 쉽게 요약한 것입니다.

Disclaimer

dCollection

이 학 석 사 학 위 논 문

Sun-induced chlorophyll fluorescence is more strongly related to absorbed photosynthetically active radiation than gross primary productivity in a rice paddy

벼논에서 관측된 태양유도 엽록소 형광은 총 일차생산성보다 군락에 의해 흡수된 광합성 유효광량과 더 강한 상관관계가 있다

August 2018

서울대학교 대학원

협동과정 농림기상학

Kaige Yang

Sun-induced chlorophyll fluorescence is more strongly related to absorbed photosynthetically active radiation than gross primary productivity in a rice paddy

UNDER THE SUPERVISION OF
PROFESSOR YOUNGYREL RYU

SUBMITTED TO THE FACULTY OF THE GRADUATE SCHOOL
OF SEOUL NATIONAL UNIVERSITY

BY
KAIGE YANG

INTERDISCIPLINARY PROGRAM IN
AGRICULTURAL AND FOREST METEOROLOGY

MAY 2018

FOR THE DEGREE OF MASTER OF SCIENCE
IN AGRICULTURAL AND FOREST METEOROLOGY

BY COMMITTEE MEMBERS

AUGUST 2018

Chair _____ (Seal)
Prof. Hyunseok Kim

Vice Chair _____ (Seal)
Prof. Youngyrel Ryu

Examiner _____ (Seal)
Prof. Kwangsoo Kim

Abstract

Sun-induced chlorophyll fluorescence (SiF) is increasingly used as a proxy for vegetation canopy photosynthesis. While ground-based, airborne, and satellite observations have demonstrated a strong linear relationship between SiF and gross primary production (GPP) at seasonal scales, their relationships at high temporal resolution across diurnal to seasonal scales remain unclear. In this study, far-red canopy SiF, GPP, and absorbed photosynthetically active radiation (APAR) were continuously monitored using automated spectral systems and an eddy flux tower over an entire growing season in a rice paddy. At half-hourly scale, strong linear relationships between SiF and GPP (R^2=0.76) and APAR and GPP (R^2=0.76) for the whole growing season were observed. We found that relative humidity, diffuse PAR fraction, and growth stage influenced the relationships between SiF and GPP, and APAR and GPP, and incorporating those factors into multiple regression analysis led to improvements up to R^2=0.83 and R^2=0.88, respectively. Relationships between LUE_p (=GPP/APAR) and LUE_f (=SiF/APAR) were inconsistent at half-hourly and weak at daily resolutions (R^2=0.24). Both at diurnal and seasonal time scales with half-hourly resolution, we found considerably stronger linear relationships between SiF and APAR than between either SiF and GPP or APAR and GPP. Overall, our results indicate that regardless of temporal resolution and time scale, canopy SiF in the rice paddy is above all a very good proxy for APAR and that therefore SiF-based GPP estimation needs to take into account relevant environmental information to model LUE_p. These findings can help develop mechanistic links between canopy SiF and GPP across multiple temporal scales.

Keyword : Sun-induced chlorophyll fluorescence (SiF); gross primary production (GPP); absorbed photosynthetically active radiation (APAR); light use efficiency (LUE_f); fluorescence yield (LUE_p)

Student Number : 2016-24596

Table of Contents

List of Figures

List of Tables

1. Introduction

1.1. Study Background

Measuring sun-induced chlorophyll fluorescence (SiF) using remote sensing platforms has opened up new opportunities to quantify the photosynthetic activity of terrestrial ecosystems (Christian et al. 2011; Porcar-Castell et al. 2014). SiF is emitted from the photosynthetic machinery in the spectral range of about 650 to 800 nm, with two peaks in the red and far-red spectral regions (Buschmann et al. 2000; Meroni et al. 2009). It is driven by absorbed photosynthetically active radiation (APAR), and shares the same excitation energy with photochemistry and non-photochemical quenching (NPQ) (Baker 2008). Therefore, the magnitude of SiF is not only closely related to the amount of APAR but also to the actual light use efficiency of photosynthesis (LUE_p), which are two crucial factors in remote sensing-based estimations of gross primary production (GPP) (Jiang and Ryu 2016; Monteith 1972; Ryu et al. 2011; Sellers 1985).

Recently, strong empirical linear relationships between canopy SiF and GPP have been widely reported at seasonal scales. These studies include retrievals from satellite (Christian et al. 2011; Guanter et al. 2012; Guanter et al. 2014; Joiner et al. 2014; Verma et al. 2017; Wagle et al. 2016; Zhang et al. 2016a), airborne (Zarco-Tejada et al. 2013a; Zarco-Tejada et al. 2013b), and ground-(Zhang et al. 2016a)based measurements (Rossini et al. 2010; Yang et al. 2017; Yang et al. 2015). Furthermore, as the revisit frequencies of satellite SiF observation increase, studies on short time scales are needed to verify results from satellite observations. The Tropospheric Emissions: Monitoring of Pollution geostationary mission, for instance, will be able to provide hourly SiF observations from space (Zoogman et al. 2017). In this case, the relationship between SiF and GPP on a diurnal time scale actually matters.

When relating canopy SiF to GPP on short temporal scales (e.g., sub-daily), however, their relationships remain unclear. First, studies on short time scales found weaker empirical linear relationships between SiF and GPP compared with seasonal scales (Cheng et al. 2013; Goulas et al. 2017; Liu et al. 2017). Cheng et al. (2013), for instance, compared GPP estimates from flux tower records with SiF retrievals from ground-based spectral measurements over four growing seasons. They found that when linking half-hourly SiF with GPP using linear regression, values of the coefficient of determination (R^2) were much lower ($R^2 \leq 0.3$) compared with values found in seasonal scale studies. Second, both model simulations (van der Tol et al. 2014; Zhang et al. 2016b) and ground based (Zhang et al. 2016b) as well as airborne measurements (Damm et al. 2015; Zarco-Tejada et al. 2016) have demonstrated that the relationship between SiF and GPP can be non-linear on short temporal scales. Zarco-Tejada et al. (2016), for example, assessed the relationships between SiF from airborne observations and field-measured leaf CO_2 assimilation over two years in a citrus crop field. They found statistically significant ($p < 0.05$) relationships between SiF and leaf carbon assimilation on a diurnal scale using second order polynomial regressions at different phenological stages throughout the season.

Observed relationships between SiF and GPP can be explained with the formulation based on the concept of light use efficiency (Monteith 1972):

$$\mathrm{GPP} = \mathrm{APAR} \times \mathrm{LUE_p} \quad (1)$$

where LUE_p is the light use efficiency of photosynthesis, which represents the efficiency of energy conversion for gross CO_2 assimilation. Similarly, SiF can be expressed as:

$$\mathrm{SiF} = \mathrm{APAR} \times \mathrm{LUE_f} \quad (2)$$

where LUE_f is the effective light use efficiency of canopy fluorescence, which accounts for both the fluorescence yield and the fraction of emitted photons escaping the canopy (Damm et al. 2015).

Currently, it remains unclear to what extent the relationship between SiF and GPP is due to APAR and/or light use efficiency at different temporal scales (Yang et al. 2015).

The relative variabilities of APAR, LUE_p and LUE_f differ strongly at short time scales. At the diurnal time scale APAR could vary from 0 to more than 2000 μmol m^{-2} s^{-1} for high LAI and sunny conditions and LUE_p is known to vary by a factor of about four to eight at the leaf-level (van der Tol et al. 2009). On the other hand, LUE_f was reported to have very conservative diurnal variation with less than a factor of two between minimum and maximum values at the leaf scale (van der Tol et al., 2014). This implies that the APAR variation is expected to strongly dominate over the LUE_f variation if diurnal dynamics are included, while GPP is known to show strong saturation with high APAR (Von Caemmerer 2000). It therefore appears plausible that for sub-diurnal temporal resolution observations at the canopy scale, SiF shows a strong linear correlation to APAR and hence the relationship between SiF and GPP will closely resemble the relationship between APAR and GPP. A consequence of this is that the slope and curvature of relationships between SiF and GPP can change on short time scales and depend strongly on the environmental conditions (Damm et al. 2015; Flexas et al. 2000) as LUE_p depends on APAR, temperature and relative humidity (Farquhar et al. 1980; van der Tol et al. 2016).

At the seasonal scale and subdiurnal temporal resolution, seasonal variation is superposed with diurnal variation which is expected to increase the dominant role

of APAR due to its large seasonal changes. If seasonal observations are considered at coarser temporal resolution such as the daily scale, however, the APAR variation is considerably reduced such that the LUE_f term is expected to play a more important role in explaining GPP and SiF relationships. Nevertheless, the effects of APAR and LUE_p could still be dominant. Furthermore, based on recent theoretical and modelling results by Yang and van der Tol (2018), the seasonal variation of LUE_f is expected to be dominated by the fraction of SiF escaping the canopy although the latter was assumed constant in previous studies (Guanter et al. 2014).

Previous results from both experimental (Miao et al., 2018) and combined experimental-modelling studies (Du et al., 2017) at the canopy level seem to partly confirm the strong SiF-APAR relationship at short time scales but were limited to either part of a growing season (Miao et al., 2018) or only studied the SiF – APAR relationship without including results on the SiF-GPP relationship (Du et al., 2017). In addition, Zhang et al. (2016a) found results consistent with our above reasoning on APAR dominance using the process-based SCOPE model (van der Tol et al. 2009). To the best of our knowledge, the responses of the SiF – GPP relationship to environmental variables such as relative humidity and temperature as well as phenology have not yet been studied quantitatively using continuous, long-term, high-temporal resolution observations at the canopy scale. While effects of diffuse PAR were studied to some degree in Yang et al. (2015), Goulas et al. (2017) and Miao et al. (2018), only sunny and cloudy days or high and low diffuse PAR fraction were distinguished and possible confounding effects such as reduced APAR on cloudy days were not taken into account.

1.2. Purpose of Research

In this study, our goal is to quantify the relationships between SiF and GPP on multiple time scales in a rice paddy. For comprehensive assessment of their relationships, we integrated a range of field observation data including canopy SiF, eddy flux measurements, canopy structure, leaf gas exchange, and meteorological variables. The main scientific questions that will be addressed in this study are: 1) is the SiF-GPP relationship indeed dominated by APAR and is this consistent on both diurnal and seasonal time scales. 2) Can we find quantitative evidence that environmental conditions and phenology significantly influence the relationship between SiF and GPP on the one hand, and LUE_p and LUE_f on the other hand in the rice paddy observations?

2. Materials and Methods

2.1. Study Site

Our study site was a rice paddy located in Cheorwon, Gangwon province, South Korea (38.2013 ℃N, 127.2506 ℃E) registered in the Korea Flux Network (KoFlux) (Figure 1). The region experiences a continental climate with hot humid summers and cold dry winters, which allows for only one growing season per year. In 2016, the mean annual temperature was 11.2 ℃; the lowest temperature was -12.2 ℃ in January and the highest temperature was 31.0 ℃ in August (Korea Meteorology Administration). Annual precipitation was 1180.9 mm, of which two-thirds typically falls during the monsoon period from June to August (Korea Meteorology Administration).

Figure 1. Location of study site and observation tower.

In the rice paddy, the predominant species was Oryza sativa L. ssp. Japonica Odea1 and it was grown intermittently irrigated, with a water depth of about 5 cm.

Soil fertilization only occurred once along with transplantation; 12.02 g N m-2 fertilizer was applied at a ratio of 18:7:9 (nitrogen: phosphoric acid: potassium). The entire growing season in 2016 lasted for around four months, from transplantation at the end of April [Day of Year (DOY), 120] to harvest in early September (DOY, 248) (Huang et al. 2018). The phenology of rice is commonly divided into three growth phases: vegetative (DOY 120 to 180); reproductive (DOY 180 to 220); and ripening (DOY 220 to harvest) (Maclean et al. 2013). The vegetative phase is characterized by a gradual increase in leaf emergence and plant height. The reproductive phase is characterized by culm elongation and a decline in tiller number. The ripening phase starts at flowering and ends when the grain is mature to be harvested. During the whole growing season, we visited the study site every one to two weeks, 14 times in total.

2.2. Sun-induced Chlorophyll Fluorescence

To continuously measure the canopy spectrum for SiF retrieval, we deployed an automated field spectroscopy system (Figure 2). The system includes as main parts a QE Pro spectrometer, two fiber optics and a 2×2 fiber optic dual switch (all components from Ocean Optics, Dunedin, FL, USA). The spectrometer covers the spectral range of 730–790 nm, with a spectral resolution of 0.17 nm, a spectral sampling interval of 0.07 nm, and a signal to noise ratio of around 1000. To avoid dark current drift, the spectrometer was housed in a National Electrical Manufacturers Association 4X enclosure, which was equipped with a thermoelectric air conditioner (400 BTU (DC); EIC Solutions, Warminster, PA, USA) and desiccant, keeping the internal temperature at 25 ℃ and the humidity mostly at a low level. Two fiber optics, pointing toward the zenith (sky) and nadir (rice canopy) directions, respectively, were mounted at around 5 m above the canopy and connected with the spectrometer through the fiber optic dual switch.

Both optics were equipped with cosine correctors (CC-3; Ocean Optics, Dunedin, FL, USA) to measure bi-hemispheric irradiance. While the downward field-of-view therefore also included the light-weight tower structure, we assume that its contribution to the total footprint is minimal and that the only effect is a small underestimation of retrieved SiF. Using a custom-written software based on Omni Driver development kits (Ocean Optics, Dunedin, FL, USA), we sequentially recorded upward and downward readings every 10 s from 06:00 to 18:00 (local solar time), and corrected for dark currents and CCD detector nonlinearity for each reading pair. Dark current correction was conducted using values from permanently dark detector pixels. We verified that dark current did not show clear spectral variation and the use of the dark pixels was therefore justified.

Several strategies were applied to assure high data quality. Following the standard method proposed by the spectrometer manufacturer, we conducted spectral calibrations using an HG-1 Mercury Calibration Source (Ocean Optics, Dunedin, FL, USA) before installing the system. Furthermore, radiometric calibration was conducted with an HL-2000-CAL Light Source (Ocean Optics, Dunedin, FL, USA) in the field around every one to two weeks. Next to the QE Pro spectrometer, we installed another spectrometer system (based on Jaz spectrometers; Ocean Optics, Dunedin, FL, USA) to record the sky and the canopy spectrum within the spectral range of 350–1033 nm. We double checked the reliability of QE Pro measurements by frequently comparing averaged downwelling and upwelling irradiance over 730-780 nm from QE Pro and Jaz.

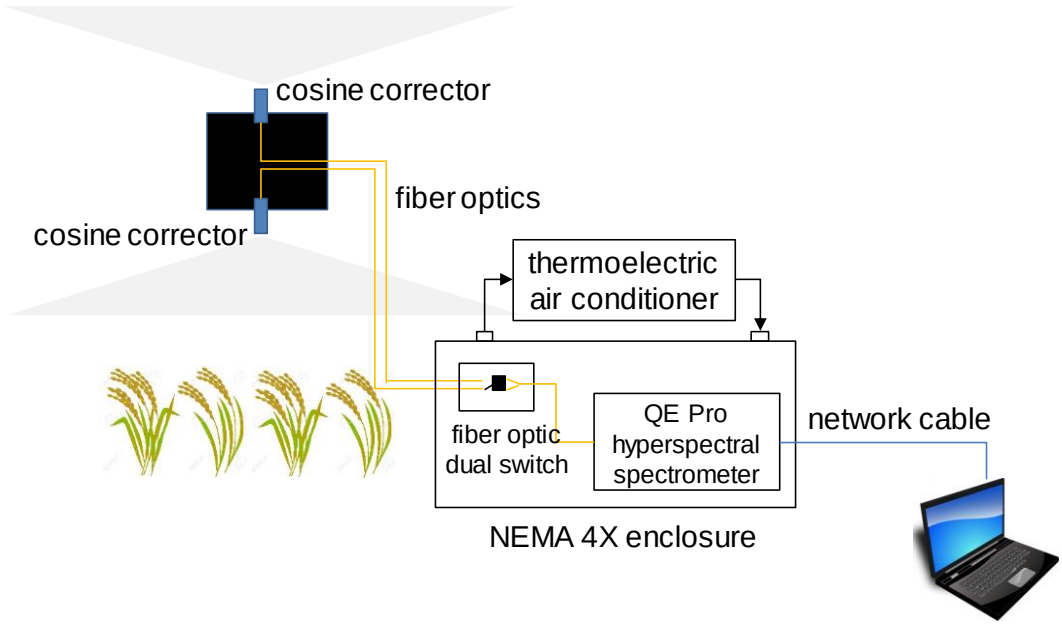

Figure 2. Schematic of the canopy SiF observation system.

We retrieved SiF values in the spectral range of 745 to 780 nm using the singular vector decomposition method (SVD) (Guanter et al. 2012; Guanter et al. 2013) (a detailed explanation is provided in the Supplementary Materials A). The fiber optic dual switch appeared to be the cause of a small spectral shift between irradiance spectra from the two fiber optics. To eliminate the influence of this spectral shift as well as artefacts due to high humidity on SiF retrieval, we used the SVD method with appropriate training data and a broad wavelength range. SiF in this study was calculated in units of irradiance based on the bi-hemispheric observation system and reported at 760 nm. We calculated LUE_f in the unit of μmol photon emitted @760nm / μmol photon absorbed @400-700nm based on the quantum nature of the physical process of fluorescence emission where one absorbed photon can lead to an emitted fluorescence photon. Daily mean SiF and LUE_f were calculated as average of the half hourly values from 08:00 to 18:00 local time.

2.3. Eddy Flux Tower

To quantify gross primary productivity (GPP), we installed a closed-path eddy covariance (EC) system at 9 m above the ground, and processed the data based on the KoFlux data processing protocol. The EC system consists of a three-dimensional sonic anemometer (Model CSAT3, Campbell Scientific Inc., Logan, UT, USA) and a closed-path infrared gas analyzer (Model LI-7200, LI-COR Inc., Lincoln, NE, USA). During the growing season, the peaks of the footprint were located about 30 m south- and northwest of the tower location, while the 80% (50%) contribution to the footprint came from distances within 300 m (100 m) from the tower during the day according to analysis using Kljun et al. (2015)'s flux footprint prediction model. To improve the data quality by eliminating undesirable data, the collected data were examined by the quality control (QC) procedure based on the KoFlux data processing protocol (Hong et al. 2009). This procedure includes the coordinate rotation (double rotation; (Mcmillen 1988)), frequency response correction (Fratini et al. 2012; Horst and Lenschow 2009), humidity correction of sonic temperature (Van Dijk et al. 2004), steady state/developed turbulent condition test (Mauder and Foken 2011), and random sampling error estimation (Finkelstein and Sims 2001). These methods were applied using EddyPro (Version 6, LI-COR Inc.) and additional QC including storage flux calculation and spike detection (Papale et al. 2006) were conducted using the KoFlux standardized data processing program (Hong et al. 2009).

After QC, the final percentage of the data retained was 48.5% for the study period. The data gaps were mostly caused by the unsatisfactory conditions for EC measurement during the nighttime and early morning (e.g., non-steady states and unfavorable developed turbulent conditions). The

missing data were gap-filled using a marginal distribution sampling method (Reichstein et al. 2005). For nighttime CO_2 flux correction and its partitioning into into GPP and ecosystem respiration (RE), we applied the friction velocity (u*) correction method with the modified moving point test method for determining u* threshold (Kang et al. 2016; Kang et al. 2017) and extrapolated nighttime values of RE into the daytime values using the RE equation (Lloyd and Taylor 1994) with a short-term temperature sensitivity of RE from the nighttime data (Reichstein et al. 2005). The gap-filling and partitioning methods were applied for each cultivation period (i.e., before transplanting, rice growing, and after harvest) separately to prevent interference effects. Daily mean GPP was calculated as average of the half hourly values from 08:00 to 18:00 local time.

2.4. Measurements of Meteorological Variables and Absorbed PAR

Environmental data were continuously collected every half hour (Figure S3). Air temperature (T_a) and relative humidity (RH) were measured at the top of the tower with a commercial instrument (HMP-35, Vaisala, Helsinki, Finland). This data was also used to quantify vapor pressure deficit (VPD). We measured total photosynthetically active radiation (PAR) and diffuse PAR (PAR_{dif}) using a quantum sensor (PQS 1; Kipp & Zonen B.V., Delft, The Netherlands) with a custom-made rotating shadow-band. Its prototype was both described and initially tested in previous studies (Michalsky et al. 1986; Michalsky et al. 1988). The value of total PAR was cross checked using incoming shortwave radiation from a CNR4 radiometer (Kipp & Zonen B.V., Delft, The Netherlands). Cloudy days were defined as daily mean fraction of PAR_{dif} larger than 50% (Yang et al. 2015).

We used three light emitting diode (LED) sensors (Ryu et al. 2010a; Ryu et al. 2014) to measure incoming PAR above the canopy, canopy reflected PAR and transmitted PAR through the canopy, respectively. We made three sets of the LED sensor system, and located each set in the footprint of the flux tower. The absorbed PAR (APAR) was then calculated as:

$$\text{APAR} = PAR_{incoming} - PAR_{reflected} - PAR_{transmitted} \quad (3)$$

We confirmed that neglecting the upwelling flux from below the canopy in Equation 3 is justified using observations from an LAI-2200 instrument (LI-COR Inc., Lincoln, NE, USA) (Figure S4). The average of APAR from three sets of the LED sensor system was used to represent the whole canopy. To remove potential measurement bias introduced by the location of LED sensors, diurnal patterns of measured APAR was adjusted and data gaps were filled with simulations from PROSAIL (Jacquemoud and Baret 1990; Jacquemoud et al. 2009; Verhoef 1984) which agreed with LAI-2200 derived fraction of APAR estimates (a detailed explanation is provided in the Supplementary Materials C). Daily environmental variables were calculated as average of the half hourly values from 08:00 to 18:00 local time.

2.5. Leaf Area Index and Maximum Carboxylation Rate

We quantified leaf area index (LAI) using a destructive approach. In each field trip, three hills of rice were randomly selected, and then all of the leaves from each hill were scanned to calculate green and yellow leaf area. A rice hill is a group of rice plants directly adjacent to each other because the seeds or seedlings were planted together (Kumar 2008). Finally, the LAI was calculated based on the total leaf area per hill and rice hill density per unit area (17.0 hills m^{-2}).

To estimate the maximum carboxylation rate (V_{cmax}), we measured A/Ci curves using an Li-6400 XT instrument (LI-COR Inc., Lincoln, NE, USA) and fitted the Farquhar-von Caemmerer-Berry model (Farquhar et al. 1980). The same same parametrization, cost function and optimization algorithm as in Dechant et al. (2017) was used for the model fitting. However, all of the four main model parameters were left unconstrained and hence fitted here and the protocol for the steps of CO_2 reference in the response curve measurements differed from Dechant et al. (2017). For better seasonal comparison, reported V_{cmax} was adjusted to 25 ℃ using literature values for activation energies from Knorr (2000) and Von Caemmerer (2000). In each field campaign, more than five sunlit leaves were randomly selected and all measurements were collected before 13:00 (local time) to avoid afternoon stomatal depression.

2.6. Statistical Analysis

Both for linear regression and Pearson correlation a significance threshold of 0.05 was used. The Analysis of Covariance (ANCOVA) toolbox and the fitlm function in MATLAB (MathWorks, Inc) were used to test if the effects of environmental conditions and growth stage on regression coefficients were significant. Negative SiF and GPP data were excluded from the analyses. Besides, outliers of LUE_p and LUE_f (beyond $\mu \pm 3\sigma$) on each day were also excluded from the diurnal relationship analysis.

3. Results

3.1. Seasonal Variations of SiF, GPP, LUE_f and LUE_p

The rice canopy showed pronounced seasonal variations in the key structural (LAI) and functional (Vcmax,25) variables (Figure 3a). Leaf Vcmax,25 first increased to 120 μmol $m^{-2}s^{-1}$ until DOY 160 and then decreased in the reproductive and ripening phases. Total LAI (including both green, yellow and senescing leaves in the ripening phase) showed a large increase in the vegetative phase with leaf emergence, and reached its maximum value (6 m^2m^{-2}) around DOY 180. Subsequently, the LAI slowly decreased in the ripening phase.

Similar seasonal trajectories were observed for SiF and GPP over the whole growing season (Figure 3c). In the seasonal course, daily mean SiF varied from almost 0 to 6 mW m-2 nm-1, and daily mean GPP varied from 0 to around 30 μmol CO2 m-2 s-1. The onset of SiF and GPP occurred on DOY 120, just after rice transplantation. In the vegetative phase, SiF and GPP showed large increases with rice canopy development until approximately DOY 180. During the reproductive phase, SiF and GPP reached their maxima and remained relatively stable except for several days when incoming PAR was low. Both SiF and GPP decreased during the ripening phase (starting approximately at DOY 220) due to leaf senescence until rice harvest. Seasonal variations in APAR explained most of the seasonal variance in SiF and GPP: we found R^2 = 0.83 and 0.85 for linear regressions between daily mean APAR with GPP and SiF (Figure 3b, Table 1). The relative RMSEs (RMSE / mean value, rRMSE) were 26% and 31% for GPP and SiF, respectively. The seasonal pattern of SiF revealed a strong linear relationship to that of GPP (R^2

= 0.87, rRMSE = 25%; Figure 4c). Besides the overall seasonal pattern, SiF also tracked day-to-day GPP variations mostly induced by varying PAR. This can be seen for the decrease of GPP around DOY 201 to 203, for example (Figure 3b, c).

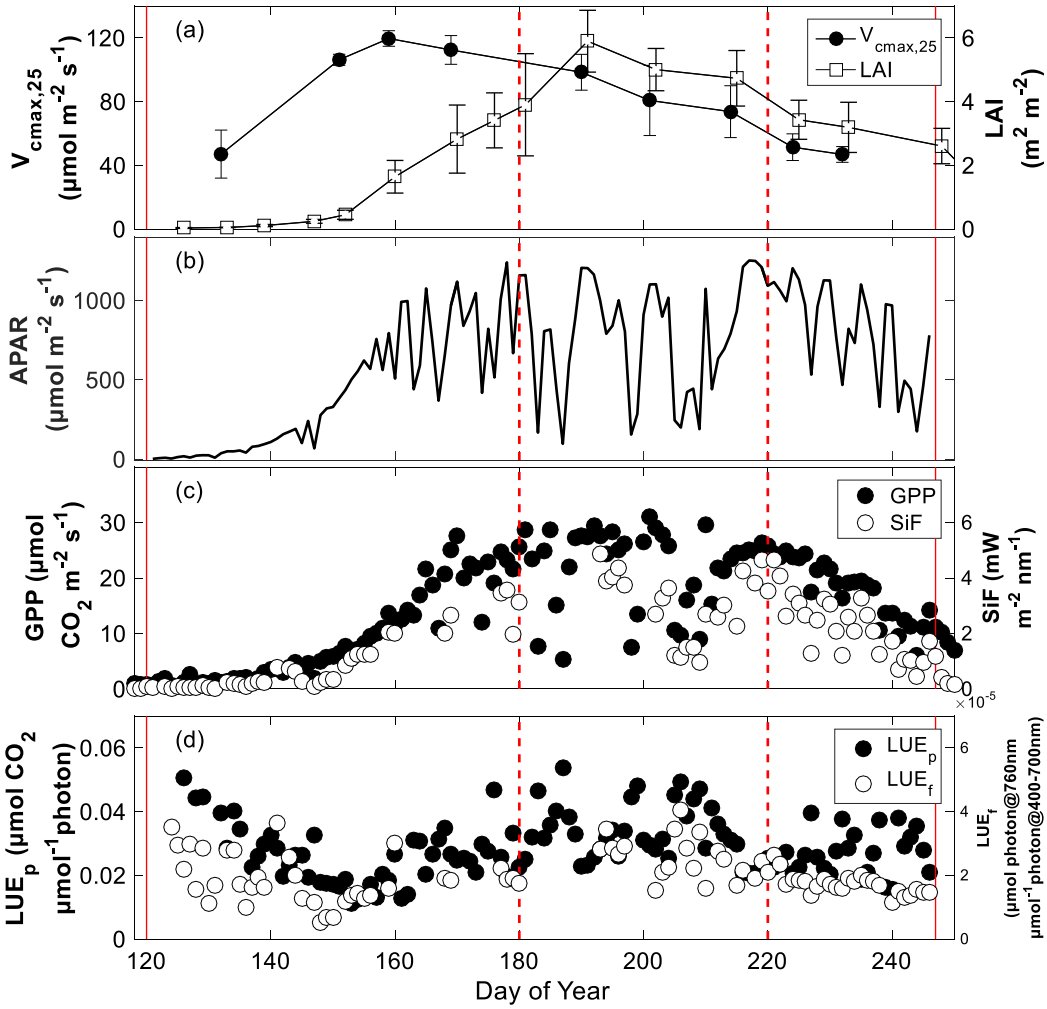

Figure 3. Seasonal variations of measured variables.

(a) Seasonal variations of field measured $V_{cmax,25}$ and LAI. Error bar indicates standard deviation of all measured samples. We added one day to DOY of LAI measurement to avoid overlapping with measurement of $V_{cmax,25}$; (b) daily mean absorbed photosynthetically active radiation (APAR); (c) daily mean gross primary productivity (GPP) and sun-induced fluorescence (SiF); (d) daily mean light use efficiency of photosynthesis (LUE_p) and light use efficiency of fluorescence

(LUE_f). Two solid red lines indicate start (DOY 120) and end (DOY 247) of the growing season, respectively. Two dashed red lines indicate beginning of reproductive and ripening phases, respectively. Daily mean values were calculated as average of half hourly values from 08:00 to 18:00 local time.

In addition, LUE_f also presented a similar seasonal pattern to LUE_p (Figure 3d) and a weak positive linear relationship with LUE_p (R^2 = 0.24, rRMSE = 27%; Table 1). Over the whole growing season, daily mean LUE_p varied from 0 to around 0.05 μmol CO_2 μmol photon^{-1}, and daily mean LUE_f from 0 to 6×10^{-5} μmol photon@760nm μmol^{-1} photon@400-700nm. The overall seasonal variations of LUE_p and LUE_f did not show strong relationships with canopy structural variables, but there appears to be a weak correlation to LAI for the time after DOY 150. Peak values of LUE_f and LUE_p generally appeared on days with low PAR (Figure 3b, d).

Table 1. Fitting goodness of linear regressions between compared variables on daily mean scale.

The coefficient of determinations (R^2), RMSE and relative RMSEs (RMSE / mean value, rRMSE) of fitted linear regressions between compared variables on daily mean scale. All R^2 values were statistically significant (p<0.05).

compared variables (X:Y)	**R^2**	**RMSE**	**rRMSE (%)**
APAR: GPP	0.83	3.98 (μmolCO_2 m^{-2}s^{-1})	26
APAR: SiF	0.85	0.56 (mWm^{-2}nm^{-1})	31
SiF: GPP	0.87	3.58 (μmolCO_2 m^{-2}s^{-1})	25
LUE_f: LUE_p	0.24	0.0077 (μmolCO_2 μmol^{-1}photon)	27

3.2. Relationships Between SiF and GPP for Different Environmental Conditions and Phenological Stages

A strong linear relationship was found between half hourly SiF and GPP over the whole growing season (R^2 = 0.76, rRMSE = 36%; Figure 4a). Considering measurements only on sunny or cloudy days showed stronger linear relationships with higherR^2 and lower rRMSE (R^2 = 0.79, rRMSE = 36% for both sunny and cloudy days; Figure 4b, c). Furthermore, compared with sunny days, the linear regression on cloudy days had a significantly steeper slope of GPP to SiF (slope = 5.89 $\pm$ 0.22 for sunny days; and slope = 6.81 $\pm$ 0.22 for cloudy days, uncertainty indicates 95% CI, Figure 4b, c). The significant differences in slopes between sunny and cloudy were also observed when forcing the linear regression to pass the origin (R^2 = 0.77, slope = 6.53 $\pm$ 0.14 for sunny days; and R^2 = 0.74, slope = 8.18 $\pm$ 0.16 for cloudy days).

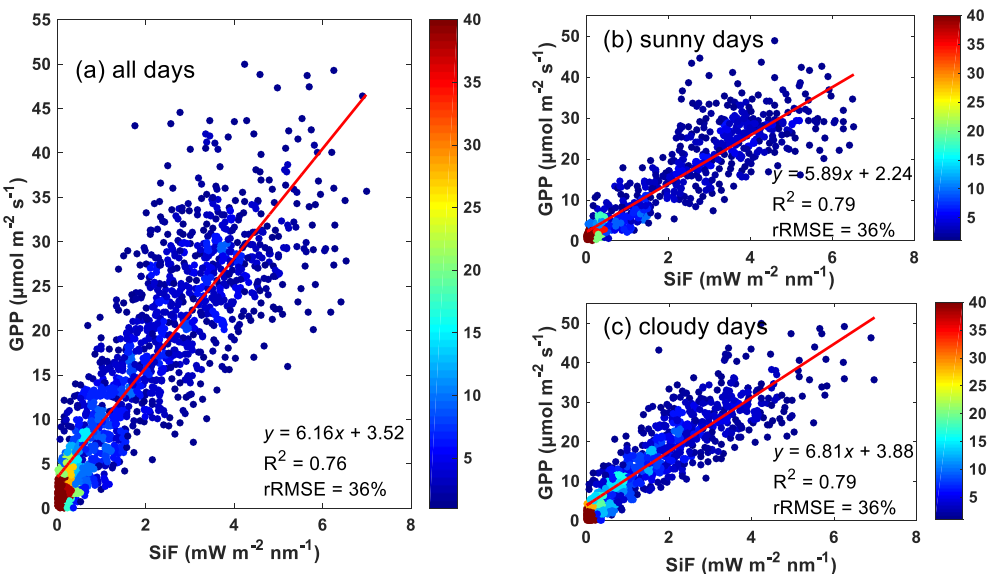

Figure 4. Scatter plots and linear regressions ($y = \mathrm{a} \times x + b$) between half hourly SiF and GPP.

(a) all illumination conditions; (b) sunny days only; and (c) cloudy days only. Linear regression lines are shown in red and regression statistics are given. R^2 and rRMSE represent the coefficient of determination and the relative RMSE (RMSE / mean) of fitted linear regressions, respectively. Color map represents point density.

The ratio of GPP to SiF showed a significant increasing trend with RH (ANCOVA $p < 0.05$, Figure 5). For a more detailed analysis, SiF and GPP data were separated according to certain ranges of T_a and RH values. In 13 out of 14 cases with available data, the linear regression fitted half hourly values of SiF and GPP well ($p < 0.05$; Table S2), with low uncertainty in individual slope values (Figure 5). Moreover, regressions results indicated that even within the relatively narrow ranges of T_a values, RH significantly impacted the slope between GPP and SiF (GPP: SiF in Figure 6), and the slope generally increased with higher RH values.

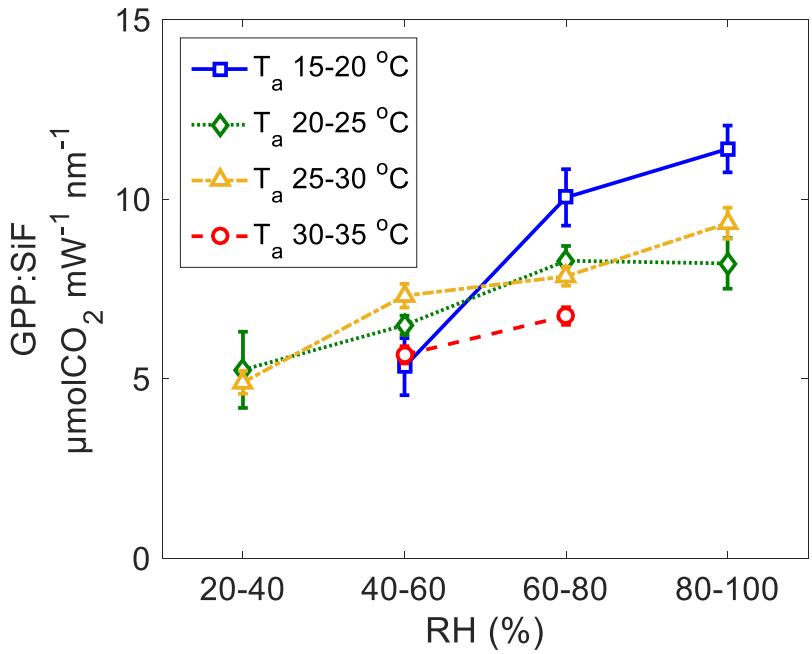

Figure 5. Slope of the linear regressions between half hourly SiF and GPP under different environmental conditions.

Slope of the linear regressions (y=a×x) symbolized by GPP: SIF between half hourly SiF and GPP over different air temperature (T_a) and relative humidity (RH) values. Uncertainty indicates 95% CI.

We analyzed the effect of the growth stage on the SiF-GPP relationship and found significant effects (Figure 6). Both slopes and offsets of the linear regression

differed significantly (ANCOVA $p < 0.05$) between growth stages with slope values showing decreasing and intercept values increasing trends over time. The largest part of the variance was explained for the vegetative stage (R^2=0.82, Figure 6a), the lowest for the reproductive stage (R^2=0.61, Figure 6b) and intermediate values for the ripening stage (R^2=0.65, Figure 6c).

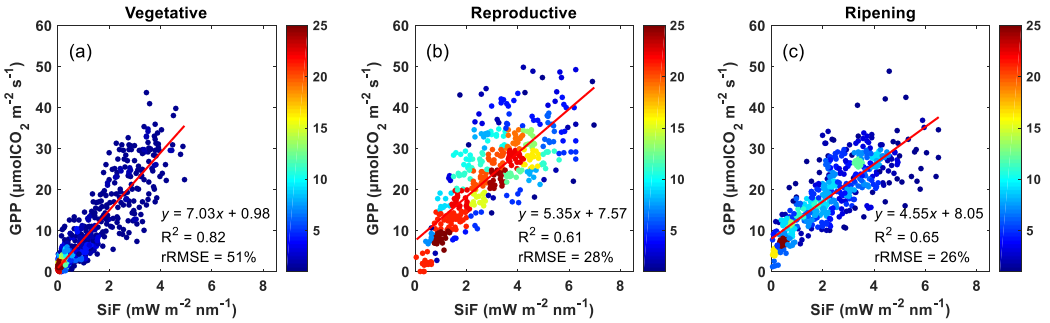

Figure 6. SiF-GPP relationships for the vegetative, reproductive and ripening growth stages of rice.

SiF-GPP relationships for the vegetative, reproductive and ripening growth stages of rice. Linear regression lines are shown in red and regression statistics are given. R^2 and rRMSE represent the coefficient of determination and the relative RMSE (RMSE / mean) of fitted linear regressions, respectively. Color map represents point density.

In order to confirm that there were indeed significant effects of RH, PAR_{dif} proportion and growth stage despite some correlation between them, we conducted a multiple regression analysis to estimate GPP from SiF including all relevant explanatory variables and interactions. The choice of the latter was based on mechanistic considerations such as the drivers of stomatal conductance (Ball et al. 1987) and the effects of diffuse radiation on LUE_p (Gu et al. 2002; Wit 1965) as well as observations from Figure 6 on the seasonal effects. The main results of this analysis are reported in Table 2 where the analogous analysis with APAR instead of SiF as main predictor is also given. We found similar improvements for single explanatory variables for the interactions of SiF with RH and SiF with PAR_{dif}

proportion (increase of total growing season R^2 from 0.74 to 0.77), while growth stage had a slightly larger effect (increase to R^2=0.80). Adding interaction effects of PAR_{dif} proportion with SiF to those of RH did only slightly improve the results despite the significance of all terms.

Table 2. Overview of regression models for GPP estimation from half-hourly data including relevant environmental variables and phenology.

The latter is incorporated in the form of growth stage (S) with three factor levels and environmental variables are relative humidity (RH) and diffuse PAR ratio ($PAR_{dif(\%)}$).The plus sign indicates additive terms while the colon indicates interaction terms. R^2 and rRMSE represent the coefficient of determination and the relative RMSE (RMSE / mean) of fitted regressions models, respectively. The best models based on either environmental predictors or LUE_p are highlighted in bold.

Explanatory terms for GPP regression model: X for SiF or APAR	**SiF** **R^2 (RMSE, rRMSE %)**	**APAR** **R^2 (RMSE, rRMSE %)**
X	0.76 (5.35, 36)	0.76 (5.42, 36)
X:LUEp	**0.82 (4.57, 31)**	**/**
X + S + X:S	0.80 (4.92, 33)	0.83 (4.58, 31)
X + X:$PAR_{dif(\%)}$	0.79 (5.07, 34)	0.84 (4.38, 29)
X + X:RH	0.79 (5.07, 34)	0.82 (4.73, 32)
X + X:$PAR_{dif(\%)}$ + X:RH	0.80 (4.96, 33)	0.86 (4.20, 28)
X + S + X:S + X:$PAR_{dif(\%)}$	0.81 (4.81, 32)	0.87 (3.95, 26)
X + S + X:S + X:RH	0.81 (4.78, 32)	0.86 (4.13, 28)
X + S + X:S + X:RH+ X:$PAR_{dif(\%)}$	0.82 (4.73, 32)	0.88 (3.80, 25)
X + S + X:S + X:RH + X:RH:S	0.82 (4.65, 31)	0.86 (4.10, 27)
X + S + X:S + X: $PAR_{dif(\%)}$ + X: $PAR_{dif(\%)}$:S	0.82 (4.70, 31)	0.87 (3.95, 26)
X + S + X:S + X:RH + X:RH:S + X:$PAR_{dif(\%)}$	**0.83 (4.61, 31)**	**0.88 (3.78, 25)**

The effect of growth stage alone was slightly larger than for RH and PAR_{dif} proportion. Combining the effects of the latter with growth stage further improved the results up to an R^2 value of 0.81, which was linked to about 14% reduction in

the GPP estimation error (RMSE) compared to the model based exclusively on SiF. While the corresponding results for APAR as main predictor were generally similar, PAR_{dif} proportion seemed to have a slightly bigger effect compared to RH and the overall error reduction was considerably larger (about 30%). For all cases with additional predictors, the APAR-based models showed better performance than the corresponding SiF-based models. The discrepancy in GPP estimation error between the best SiF- and APAR-based models was considerable (rRMSE of 31% and 25%, respectively), while the difference in RMSE for the simplest models was small (< 1%). Furthermore, we also found that the model based on the product of SiF with LUE_p outperformed the best SiF-based model with environmental and growth stage interaction terms. If not indicated otherwise in the tables, all interaction terms were significant. We used the Akaike information criterion (AIC) to verify that the improvement obtained by adding more predictor terms to the models was not offset by the corresponding reduction in degrees of freedom (results not shown).

3.3. Diurnal Relationships Between SiF and GPP

On the diurnal scale for individual date, SiF showed linear relationships with GPP over two thirds of individual days over the growing season (Figure 7c), and their relationships were predominantly driven by APAR (Figure 7a, b). We analyzed the diurnal relationships between APAR and GPP, APAR and SiF, SiF and GPP, as well as LUE_f and LUE_p on individual days over the whole growing season. Only days with more than 50% observations from 08:00 to 18:00 local time were considered. Among 126 available days, GPP showed significant linear relationships to APAR on 81% of individual days (R^2: 0.19-0.96, Figure 8a). More than 70% of the days that had no significant APAR-GPP relationship occurred in the early stages of the growing season (DOY <143), which was characterized by

low numbers of available GPP measurements per day. Over the whole growing season, 90 days were available for SiF data. Around 84% of those days showed significant linear APAR-SiF relationships (Figure 8b), which was a slightly higher fraction than that for GPP, and their R^2 ranged from 0.20 to 0.98. The mean R^2 over days with significant relationship was 0.65 for APAR-GPP, and 0.76 for APAR-SiF. Furthermore, we found significant linear relationships between SiF and GPP on around 70% of individual days (Figure 8c), and their R^2 ranged from 0.19 to 0.92, with a mean value of 0.60.

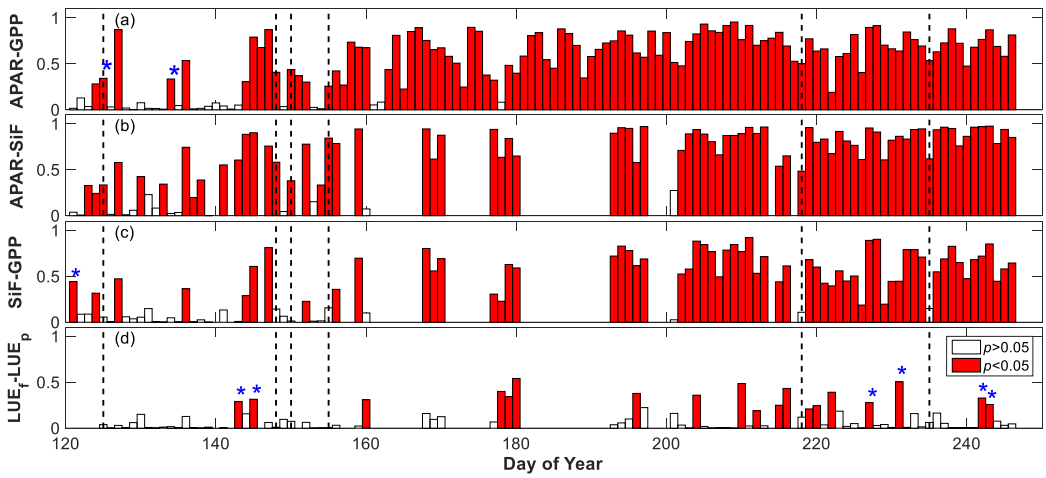

Figure 7. Coefficients of determinations (R2) of linear regressions ($y = \mathrm{a} \times x + \mathrm{b}$) between half-hourly measurements.

(a) APAR and GPP; (b) APAR and SiF; (c) SiF and GPP; and (d) LUE_f and LUE_p on individual days over the whole growing season. Vertical dashed lines represent individual days when SiF is not significantly related to GPP, while both SiF and GPP show significant linear relationships with APAR. Blue '*' indicates negative correlations between compared variables.

Among 90 available days for SiF and GPP, 27 days of them presented no significant linear relationship between SiF and GPP (Figure 8c). Most of these instances (74%) were from days before DOY 150 which also showed no significant relationships between APAR with either GPP or SiF. Besides, there were cases for which even though both SiF and GPP were linearly related to APAR, the absence

of strong relationships between LUE_f and LUE_p seemed to lead to weak SiF-GPP relationships (see individual days with vertical dashed lines in Figure 8). Over the whole growing season, LUE_f only showed linear relationships with LUE_p on around 22% of individual days ($p < 0.05$, Figure 8d), and their R^2 ranged from 0.19 to 0.54, with a mean value of 0.34. In addition, on around one third of the days with significant relationships, LUE_f showed negative relationships with LUE_p.

3.4. Relationships Between LUE_f and LUE_p on Clear Sky Days

To investigate the effects of phenology on LUE_f and LUE_p relationships, clear sky days (daily mean proportion of beam direct PAR > 0.7) from three growth phases were chosen (10, 12, 8 days in vegetative, reproductive and ripening phases, respectively), and the mean diurnal courses of LUE_f and LUE_p were calculated (Figure 8a–f). We then analyzed diurnal correlations between LUE_f with LUE_p (Figure 8g–i) over different phenological phases. Across the three growth phases, LUE_p followed a typical diurnal cycle under clear sky conditions, where values showed a steady decrease during morning hours and a subsequent increase after solar noon (13:00 local time) (Figure 8a–c). In the vegetative and reproductive phases, we observed qualitatively similar diurnal courses for LUE_f and LUE_p (Figure 8d, e), which decreased from early in the morning until solar noon, and slowly increased afterwards. Significant LUE_f-LUE_p relationships were observed in the vegetative ($r = 0.54$) and reproductive ($r = 0.82$) phases (Figure 8g–i). In the ripening phase, LUE_f and LUE_p showed decoupled diurnal variations: in contrast to LUE_p, the diurnal course of LUE_f was highly asymmetric with almost constant values in the morning and showed qualitatively similar behavior as LUE_p only in the afternoon (Figure 8c). This resulted in an overall non-significant relationship between LUE_f and LUE_p in the ripening stage, while the relationship for only the afternoon hours was strong (r =0.95) and significant (Figure 8i).

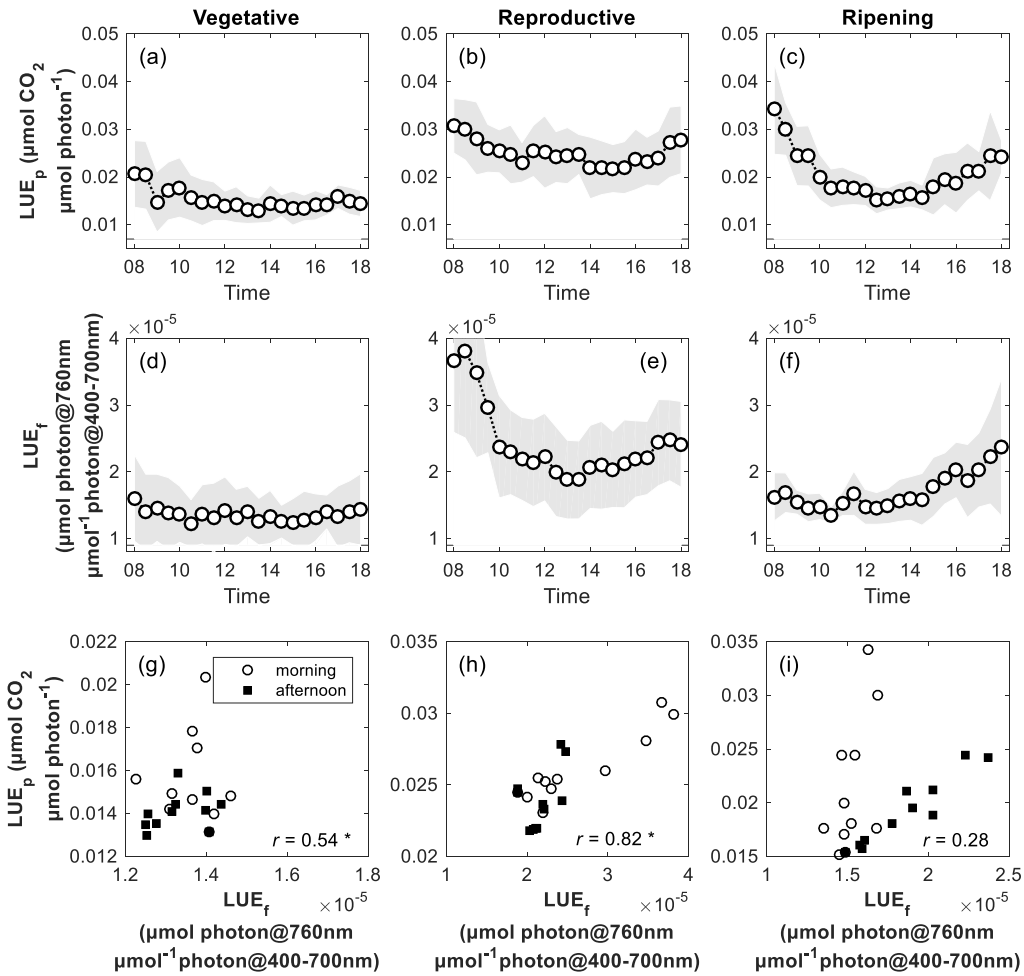

Figure 8. Averaged diurnal courses on clear sky days (daily mean direct PAR proportion > 0.7).

(a-c) LUE_p and (d–f) LUE_f (circles represent averaged values, and shaded bands represent standard deviation), as well as correlations between averaged LUE_p and LUE_f over the whole day at different growing stages (g–i). In (g–i), '*r*' denotes Pearson correlation. From left to right, each column represents vegetative, reproductive, and ripening phase, respectively.

To understand the relationships of LUE_f and LUE_p with relevant environmental variables across different phenological stages, we applied partial correlation analysis for half-hourly APAR, PAR_{dif} proportion, and VPD data on the dates that were used in Figure 8. In contrast to LUE_f, LUE_p was significantly and

positively correlated to PAR_{dif} proportion in all phenological stages. LUE_f showed significant negative correlations to APAR except for the vegetative stage where the correlation was positive. In the ripening stage, a significant positive correlation was found between VPD and LUE_f, while the correlation was always negative for LUE_p in all the three growing stages.

Table 3. Partial correlations between LUE and the environmental variables.

Partial correlations between half-hourly LUE (LUE_p or LUE_f) and the environmental variables: absorbed PAR (APAR), diffuse PAR proportion, and vapor pressure deficit (VPD) between 0800hh and 1800hh on clear sky days (daily mean direct PAR proportion > 0.7). Bold font indicates significant correlation (p <0.05).

Growing phase		**APAR**	**Diffuse PAR proportion**	**VPD**
Vegetative	LUE_p	0.14	0.11	**-0.42**
	LUE_f	**0.59**	**0.17**	-0.03
Reproductive	LUE_p	**-0.19**	**0.31**	**-0.27**
	LUE_f	**-0.31**	0.07	**-0.35**
Ripening	LUE_p	**-0.32**	**0.58**	-0.12
	LUE_f	**-0.23**	**0.20**	**0.53**

4. Discussion

In this study, we retrieved SiF values from automatic ground-based observations and investigated the relationships between canopy SiF and GPP from eddy covariance measurements at seasonal and diurnal scales in a rice paddy. More importantly, we analyzed how environmental conditions influenced the relationship between SiF and GPP, as well as explored the response of LUE_f and LUE_p to environmental variations at different rice phenological stages. We believe this is the first study that reported continuous observations of GPP and SiF over the whole growing season in rice paddy.

4.1. Relationships Between SiF and GPP on Different Temporal Scales

At the seasonal scale, daily mean SiF tracked temporal variations of daily mean GPP well (Figure 3c), and showed a strong linear relationship with GPP, which is comparable to APAR (R^2 = 0.83, rRMSE = 26% for APAR-GPP; R^2 = 0.87, rRMSE = 25% for SiF-GPP. Table 1). This finding demonstrated that the linear relationship between seasonal patterns of SiF and GPP was mostly explained by the strong APAR-SiF relationship (R^2 = 0.85, Table 1), which is similar to the result of Yang et al. (2015) who observed higher SiF-APAR (R^2 = 0.79) than SiF-GPP (R^2 = 0.73) correlation. Nevertheless, we also found a weak but significant relationship between daily mean of LUE_f and LUE_p over the growing season (p < 0.05, R^2 = 0.24, Figure 3d, Table 1). This finding is consistent with Yang et al. (2015) that found a slightly higher correlation at daily temporal resolution (R^2 = 0.38). Rossini et al. (2010), however, found a strong linear relationship between LUE_f and LUE_p (R^2 = 0.74) in a rice paddy with data from 15 measurement campaigns over two years, and demonstrated that this relationship could be used to considerably improve LUE-based GPP models.

On the diurnal scale, we found that SiF was linearly related with GPP on more than two thirds of individual days, with a mean R^2 value of 0.60 (Figure 7c). Besides, similar to the seasonal scale, the SiF-GPP relationship on the diurnal scale was also predominantly explained by APAR (Figure 7). In general, APAR performed slightly better than SiF in tracking diurnal variations in GPP, which had more days with significant linear relationships (81% for APAR-GPP, and 70% for SiF-GPP) and a slightly higher mean value of explained variance (R^2 = 0.65 and 0.60 for APAR and SiF, respectively). Moreover, the significant linear relationships between LUE_f and LUE_p were only found on 22% with a rather low mean value (R^2=0.34). The higher correlation of LUE_f and LUE_p at the seasonal scale with daily temporal resolution implies that the effects of more seasonally varying properties such as pigment contents, photosynthetic capacity and canopy structure on LUE_p is better captured by SiF than the effects of short-term variations of environmental conditions on LUE_p. The poorer performance of SiF to track GPP in the early growing stage might be associated with the decoupled diurnal variation of LUE_f and LUE_p in most of the days (> 80%) (Figure 7d).

While both model simulations and ground based observations have demonstrated that relationships between SiF and GPP tend to be more linear at coarser temporal scale (Damm et al. 2015; Goulas et al. 2017; Zhang et al. 2016b), we found that the linear relationships between half hourly SiF and GPP were comparable to the corresponding daily relationships (R^2 = 0.76 for half hourly SiF and GPP, Figure 4a; R^2 = 0.87 for daily mean SiF and GPP, Table 1). Zhang et al. (2016b), for instance, reported that the R^2 of the linear regression between SiF-GPP at the Harvard Forest increased from 0.42 over 0.74 to 0.84 after aggregating from hourly over daily to 16-days. Both results are not contradictory when considering the variation of GPP to APAR. The linearization effect is caused

mainly by the decrease of APAR values due to averaging such that the saturation effects for GPP tend to get weaker or even entirely disappear (Damm et al. 2015; Zhang et al. 2016b), which is in accordance with well-known observations that temporal averaging tends to linearize the response between GPP and APAR (Baldocchi and Amthor 2001; Ruimy et al. 1995). However, in the rice paddy, saturation of GPP with APAR and GPP with SiF was not as clearly observed at half hourly time scale (linear regression: $R^2 = 0.73$, rRMSE = 34% for APAR-GPP) as in other studies (e.g. Zhang et al., 2016a). Hence the mechanism of the linearization effect described above could only lead to moderate improvements in the linear SiF-GPP relationship on daily scale ($R^2 = 0.85$, rRMSE = 26%) that were comparable to the change from daily to 16 day averages in Zhang et al. (2016a). Addition of fertilizer and the erectophile canopy of rice might explain the absence of strong saturation effects of GPP with APAR.

4.2. Effects of Environmental Factors and Phenology on the Relationship Between SiF and GPP

Half hourly SiF was strongly and linearly related to half hourly GPP over the whole growing season in the rice paddy ($R^2 = 0.76$), but the slope of their linear regressions was found to vary depending on environmental conditions such as PAR_{dif} fraction and RH (Figures 4, 5, S4) as well as the growth stage (Figure 6).

We found that sky conditions had two effects on the relationship between SiF and GPP. First, the GPP to SiF ratio was higher on cloudy days (Figure 4b, c). Greater proportion of diffuse light that allows more evenly distributed light over different canopy layers is well known to increase canopy LUE_p by enhancing photosynthesis in shaded leaves which are light limited (Alton et al. 2007; Gu et al. 2003). The effects of diffuse light on LUE_f should also be considered in this context.

According to the escape ratio formula for far-red SiF by Yang and van der Tol (2018), LUE_f is expected to increase with PAR_{dif} fraction due to the increase in the canopy near-infrared reflectance (e.g. Ryu et al., 2010a) while the canopy interceptance is not much affected for a closed canopy. This effect, however, would tend to decrease the GPP:SiF ratio on cloudy days, which is not the observed pattern and hence, the LUE_p effects seem to dominate over LUE_f effects in the response to diffuse light. Second, the linear relationship was stronger considering only sunny or cloudy days separately, while the correlation on sunny and cloudy days are comparable (Figure 4b, c). In contrast to our result, Zhang et al. (2016b) also found that the SiF-GPP relationship became stronger during sunny days in Harvard forest (R^2=0.79 for sunny, R^2=0.74 for cloudy) and Miao et al. (2018) confirmed this tendency for soybean (R^2=0.65 for sunny, R^2=0.52 for cloudy). Goulas et al. (2017), however, found that in a winter wheat field the relationship between half-hourly SiF and GPP slightly weakened if measurements under sunny conditions were considered. The canopy structure of a rice paddy, deciduous forest, and winter wheat field differ substantially in terms of LAI and leaf inclination angle but effects of PAR_{dif} were observed in all cases. Our multiple regression analysis also confirmed that incorporating PAR_{dif} proportion with SiF improved GPP prediction (Table 2). Overall, these findings suggest that at the canopy scale, not only light intensity but also the PAR_{dif} fraction should be considered when linking SiF to GPP.

Furthermore, we found that the ratio of GPP to SiF generally increased with RH in the rice paddy (Figure 5). This trend was generally consistent across each phenological stage (data not shown). A C3 leaf biochemical fluorescence model predicted that GPP:SiF ratio increased with RH and T_a (van der Tol et al. 2014) (Figure 9). We used the model with diverse ranges in PAR and $V_{cmax,25}$, which all produced increasing trends of the GPP:SiF ratio with RH, which supports our in-

situ data. The model results revealed that increase of RH led to higher stomatal conductance, and hence intercellular CO_2 concentration, and GPP whereas SiF was relatively insensitive to RH. This implies that GPP:SiF relationship against RH is dominantly controlled by LUE_p, not LUE_f. Multiple regression analysis also confirmed that combining RH with SiF improved GPP prediction (Tables 2, 3). There is still ongoing debate whether RH or VPD is the direct driver of stomatal limitation of photosynthesis (e.g.) (Sato et al. 2015). We therefore compared multiple regression analyses using either RH or VPD and found consistent results with very small differences. This can also be attributed to the high correlation of RH and VPD for our dataset (R^2=0.78).

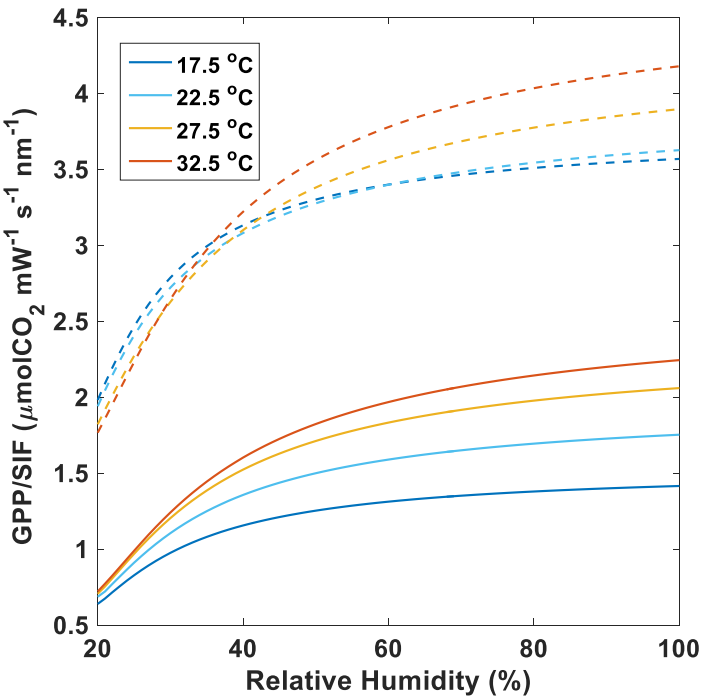

Figure 9. Simulated leaf-level values of the ratio of photosynthesis (GPP) to sun-induced chlorophyll fluorescence (SiF) against relative humidity and temperature. Data presented here used a C3 leaf biochemical photosynthesis model (van der Tol et al. 2014) at $V_{cmax,25}$=80 µmol m^{-2} s^{-1}, CO_2=400 ppm, O_2=21%. PAR=1500 µmol m^{-2} s^{-1} for solid lines and PAR = 500 µmol m^{-2} s^{-1} for dashed lines.

We found clear evidence of a seasonally changing SIF-GPP relationship (Figure 6), which could be related to canopy structure effects affecting the fraction of emitted SiF escaping the canopy. Recently published results including both simulations and field observations showed strong effects of canopy structure on the APAR-SiF relationship (Du et al. 2017), which in turn will also affect the GPP-SiF relationship. In the rice paddy, mean leaf inclination angle, which was measured using a leveled digital camera photography method (Ryu et al. 2010b), changed in the course of the growing season with variations from 50 to 70 degrees (data not shown) and this together with changes in LAI as well as leaf senescence in the ripening stage is expected to affect the fraction of SiF escaping the canopy. Multiple regression analysis confirmed that incorporating phenological stage information into SiF improved GPP predictions (Tables 2, 3). Therefore, accounting for the escape fraction that depends on canopy structure may be necessary to improve SiF-based GPP estimation. Recently, a simplified approach to calculate the escape fraction was presented by Yang and van der Tol (2018) that seems promising for future application. Furthermore, anisotropy effects have been shown to play a role also for SiF (Liu et al. 2016; Pinto et al. 2017). While a study of the latter goes beyond the scope of our work, they should be addressed in more detail in the future.

4.3. Effects of Environmental Factors and Phenology on Light Use Efficiencies on Clear Sky Days

Studying the relationships of LUE_f and LUE_p on clear sky days is important as airborne campaigns are typically conducted on such days and satellite data acquired on cloudy days tend to suffer from data quality limitations. LUE_f and LUE_p responded differently to APAR and VPD on clear sky days across vegetative, reproductive, and ripening stages (Table 3). We found that LUE_f showed positive

correlation to APAR only in the vegetative stage while correlations were negative in the other stages (Table 3). Leaf level simulation using the SiF leaf model (van der Tol et al. 2014) implemented in the widely used SCOPE model (van der Tol et al. 2009) reported that LUE_f increased then decreased with APAR, and with greater $V_{cmax,25}$, the inflection point moved towards right (i.e. higher APAR) (Frankenberg and Berry 2018; van der Tol et al. 2014). In the vegetative stage, $V_{cmax,25}$ approached peak values around 120 μmol m^{-2} s^{-1} and APAR was relatively lower than the other stages (Figure 3). We assume the higher $V_{cmax,25}$ with lower APAR led to the positive correlation between LUE_f and APAR (Figure 3, Table 3). In the reproductive and ripening stages, $V_{cmax,25}$ gradually decreased while keeping a high level of APAR, which is likely to explain the negative correlations between LUE_f and APAR. The photosynthesis model based on Farquhar et al. (1980) and Collatz et al. (1991) implemented in SCOPE predicted a consistent decrease of LUE_p with APAR regardless of $V_{cmax,25}$ values. This agreed very well with our result that LUE_p was negatively correlated to APAR across all phenological stages that experienced a large seasonal variation in $V_{cmax,25}$ (Table 3, Figure 3a). While the latter finding is expected to also hold at the canopy level (Knohl and Baldocchi 2008), the apparently good agreement of leaf-level LUE_f -APAR relationships with canopy observations is somewhat surprising as the low APAR values at the beginning of the season are due to low overall LAI and not due to low APAR for individual leaves. That is, individual leaves might be light saturated, which implies mostly negative correlation of LUE_f with APAR at the leaf-level. Therefore, an overall negative correlation of LUE_f with APAR might also be expected at the canopy level. Further experimental studies and simulations are needed to investigate this.

We found VPD was positively correlated only to LUE_f in the ripening stage (Table 3). The LUE_p:LUE_f ratio substantially decreased in the afternoon of the ripening stage (Figure 8i) indicating that, relatively speaking, the rice canopy

converted a larger proportion of APAR into SiF than it used for photochemical reactions compared to the morning hours. In the ripening stage, low values of $V_{cmax,25}$ and greater VPD in the afternoon would lead more of the absorbed energy to be dissipated in processes other than photosynthesis such as NPQ and fluorescence. Diurnal hysteresis effects involving changes in the LUE_p:LUE_f ratio were previously reported (Porcar-Castell et al. 2014), although with lower LUE_f in the afternoon in contrast to our findings. However, leaf senescence was shown to affect LUE_p and NPQ in previous studies (Lu et al. 2001; Wingler et al. 2004) and this might also affect the diurnal relationships. We are cautious in our interpretation as the canopy includes up to 30% yellow leaves in the ripening stage (data not shown), which still partly contribute to APAR but do not play any direct role in photochemistry, fluorescence and NPQ. However, they can contribute to changes in the SiF escape fraction and thus modify the effective LUE_f, which could not be corrected for with our observations.

4.4. Synthesis and Implications of Statistical Analysis of APAR-GPP, SiF-GPP and LUE_p-LUE_f Relationships

Overall, we found that for 30 min temporal resolution, APAR-based models outperformed SiF-based models for GPP estimation in all cases, both for the whole growing season (Table 2) and for the separate growth stages (results not shown). Furthermore, the improvements when including environmental and growth stage effects were substantially larger for APAR-based than SiF-based models (Tables 2 and 3). In addition, we found that the LUE_f -LUE_p relationship was very weak at high temporal resolution and that using the product of SiF with LUE_p rather than SiF directly considerably decreased the GPP estimation errors (Tables 2, 3). The above-mentioned findings all suggest that SiF observed in the rice paddy should be considered primarily as proxy for APAR rather than a more direct link to

photosynthesis that contains considerable information on LUE_p. This is consistent with the experimental results of Miao et al. (2018) for soybean that reported stronger relationships between SiF and APAR than SiF and GPP at half-hourly temporal resolution. All these findings seem to contradict other studies that reported canopy escaping SiF as proxy for photosynthetic electron transport rate (ETR), which is the product of APAR with the efficiency of photosystem II (Guan et al. 2016; Zhang et al. 2014).

Our results have important implications for SiF-based GPP estimation at large scales. From the observation that canopy-level retrieved SiF in the rice paddy contains almost exclusively information on APAR, it follows that the SiF-GPP relationship corresponds to the APAR-GPP relationship and hence needs to be modified for well-known LUE_p effects related to RH or VPD, PAR_{dif}, temperature and phenology (Jenkins et al. 2007; Knohl and Baldocchi 2008; Running et al. 2004). Satellite remote sensing enables us to monitor those key variables such as PAR_{dif} proportion (Figure 4) (Ryu et al. 2018), RH (Figure 5) (Hashimoto et al. 2008; Ryu et al. 2008), and phenology information (Figure 6) such as LAI, clumping index, and mean leaf angle (He et al. 2016; Myneni et al. 2002; Zou and Mõttus 2015) across multiple spatial and temporal scales, which offers new opportunities for monitoring GPP through SiF and LUE_p.

5. Conclusion

We investigated the relationships of SiF retrieved from high-resolution spectrometer observations with GPP over an entire growing season in a rice paddy. We found strong linear relationships between SiF and GPP both at half-hourly and daily temporal resolutions, but that these were almost exclusively driven by the strong relationships between SiF and APAR. On the diurnal scale, the SiF-APAR relationships were considerably stronger than the SiF-GPP relationships. The relationships between LUE_f and LUE_p were generally weak and inconsistent on both seasonal and diurnal scales at high temporal resolution, but showed clear dependence on environmental factors as well as plant phenology on clear sky days. We demonstrated that including effects of RH and the diffuse PAR fraction as well as growth stage into statistical models of SiF- and APAR-based GPP estimation considerably improved the performance. This is consistent with commonly used approaches to model photosynthetic light use efficiency based on environmental variables and indicates that at least at high temporal resolution, canopy-level SiF for rice is essentially only a good proxy for APAR and does not contain much relevant information on LUE_p. This has important implications for future studies aiming at using SiF information to improve large scale GPP estimation, no matter if process-based or empirical approaches are applied.

References

Alton, P.B., North, P.R., & Los, S.O. (2007). The impact of diffuse sunlight on canopy light-use efficiency, gross photosynthetic product and net ecosystem exchange in three forest biomes. *Global Change Biology, 13*, 776-787

Baker, N.R. (2008). Chlorophyll Fluorescence: A Probe of Photosynthesis In Vivo. *Annual Review of Plant Biology, 59*, 89-113

Baldocchi, D.D., & Amthor, J.S. (2001). Canopy photosynthesis: history. *Terrestrial Global Productivity; Academic Press: New York, NY, USA*, 9-31

Ball, J.T., Woodrow, I.E., & Berry, J.A. (1987). A model predicting stomatal conductance and its contribution to the control of photosynthesis under different environmental conditions. *Progress in photosynthesis research* (pp. 221-224): Springer

Buschmann, C., Langsdorf, G., & Lichtenthaler, H.K. (2000). Imaging of the blue, green, and red fluorescence emission of plants: An overview. *Photosynthetica, 38*, 483-491

Cheng, Y.B., Middleton, E.M., Zhang, Q.Y., Huemmrich, K.F., Campbell, P.K.E., Corp, L.A., Cook, B.D., Kustas, W.P., & Daughtry, C.S. (2013). Integrating Solar Induced Fluorescence and the Photochemical Reflectance Index for Estimating Gross Primary Production in a Cornfield. *Remote Sensing, 5*, 6857-6879

Christian, F., B., F.J., John, W., Grayson, B., S., S.S., Jung-Eun, L., C., T.G., Andr é, B., Martin, J., Akihiko, K., & Tatsuya, Y. (2011). New global observations of the terrestrial carbon cycle from GOSAT: Patterns of plant fluorescence with gross primary productivity. *Geophysical Research Letters, 38*

Collatz, G.J., Ball, J.T., Grivet, C., & Berry, J.A. (1991). Physiological and Environmental-Regulation of Stomatal Conductance, Photosynthesis and Transpiration - a Model That Includes a Laminar Boundary-Layer. *Agricultural and Forest Meteorology, 54*, 107-136

Damm, A., Guanter, L., Paul-Limoges, E., van der Tol, C., Hueni, A., Buchmann, N., Eugster, W., Ammann, C., & Schaepman, M.E. (2015). Far-red sun-induced chlorophyll fluorescence shows ecosystem-specific relationships to gross primary production: An assessment based on observational and modeling approaches. *Remote Sensing of Environment, 166*, 91-105

Dechant, B., Cuntz, M., Vohland, M., Schulz, E., & Doktor, D. (2017). Estimation of photosynthesis traits from leaf reflectance spectra: Correlation to nitrogen content as the dominant mechanism. *Remote Sensing of Environment, 196*, 279-292

Du, S.S., Liu, L.Y., Liu, X.J., & Hu, J.C. (2017). Response of Canopy Solar-Induced Chlorophyll Fluorescence to the Absorbed Photosynthetically Active Radiation Absorbed by Chlorophyll. *Remote Sensing, 9*, 911

Farquhar, G.D., von Caemmerer, S., & Berry, J.A. (1980). A biochemical model of photosynthetic CO2 assimilation in leaves of C3 species. *Planta, 149*, 78-90

Finkelstein, P.L., & Sims, P.F. (2001). Sampling error in eddy correlation flux measurements. *Journal of Geophysical Research-Atmospheres, 106*, 3503-3509

Flexas, J., Briantais, J.M., Cerovic, Z., Medrano, H., & Moya, I. (2000). Steady-state and maximum chlorophyll fluorescence responses to water stress in grapevine leaves: A new remote sensing system. *Remote Sensing of Environment, 73*, 283-297

Frankenberg, C., & Berry, J. (2018). Solar Induced Chlorophyll Fluorescence: Origins, Relation to Photosynthesis and Retrieval. *Reference Module in Earth Systems and Environmental Sciences: Comprehensive Remote Sensing* (pp. 143-162). Oxford: Elsevier

Fratini, G., Ibrom, A., Arriga, N., Burba, G., & Papale, D. (2012). Relative humidity effects on water vapour fluxes measured with closed-path eddy-covariance systems with short sampling lines. *Agricultural and Forest Meteorology, 165*, 53-63

Goulas, Y., Fournier, A., Daumard, F., Champagne, S., Ounis, A., Marloie, O., & Moya, I. (2017). Gross Primary Production of a Wheat Canopy Relates Stronger to Far Red Than to Red Solar-Induced Chlorophyll Fluorescence. *Remote Sensing, 9*, 97

Gu, L., Baldocchi, D., Verma, S.B., Black, T., Vesala, T., Falge, E.M., & Dowty, P.R. (2002). Advantages of diffuse radiation for terrestrial ecosystem productivity. *Journal of Geophysical Research: Atmospheres, 107*

Gu, L., Baldocchi, D.D., Wofsy, S.C., Munger, J.W., Michalsky, J.J., Urbanski, S.P., & Boden, T.A. (2003). Response of a deciduous forest to the Mount Pinatubo eruption: enhanced photosynthesis. *Science, 299*, 2035-2038

Guan, K., Berry, J.A., Zhang, Y., Joiner, J., Guanter, L., Badgley, G., & Lobell, D.B. (2016). Improving the monitoring of crop productivity using spaceborne solar-induced fluorescence. *Globle Change Biology, 22*, 716-726

Guanter, L., Frankenberg, C., Dudhia, A., Lewis, P.E., Gómez-Dans, J., Kuze, A., Suto, H., & Grainger, R.G. (2012). Retrieval and global assessment of terrestrial chlorophyll fluorescence from GOSAT space measurements. *Remote Sensing of Environment, 121*, 236-251

Guanter, L., Rossini, M., Colombo, R., Meroni, M., Frankenberg, C., Lee, J.E., & Joiner, J. (2013). Using field spectroscopy to assess the potential of statistical approaches for the

retrieval of sun-induced chlorophyll fluorescence from ground and space. *Remote Sensing of Environment, 133*, 52-61

Guanter, L., Zhang, Y., Jung, M., Joiner, J., Voigt, M., Berry, J.A., Frankenberg, C., Huete, A.R., Zarco-Tejada, P., Lee, J.-E., Moran, M.S., Ponce-Campos, G., Beer, C., Camps-Valls, G., Buchmann, N., Gianelle, D., Klumpp, K., Cescatti, A., Baker, J.M., & Griffis, T.J. (2014). Global and time-resolved monitoring of crop photosynthesis with chlorophyll fluorescence. *Proceedings of the National Academy of Sciences, 111*, E1327-E1333

Hashimoto, H., Dungan, J.L., White, M.A., Yang, F., Michaelis, A.R., Running, S.W., & Nemani, R.R. (2008). Satellite-based estimation of surface vapor pressure deficits using MODIS land surface temperature data. *Remote Sensing of Environment, 112*, 142-155

He, L., Liu, J., Chen, J.M., Croft, H., Wang, R., Sprintsin, M., Zheng, T., Ryu, Y., Pisek, J., Gonsamo, A., Deng, F., & Zhang, Y. (2016). Inter- and intra-annual variations of clumping index derived from the MODIS BRDF product. *International Journal of Applied Earth Observation and Geoinformation, 44*, 53-60

Hong, J.-K., Kwon, H.-J., Lim, J.-H., Byun, Y.-H., Lee, J.-H., & Kim, J. (2009). Standardization of KoFlux eddy-covariance data processing. *Korean Journal of Agricultural and Forest Meteorology, 11*, 19-26

Horst, T.W., & Lenschow, D.H. (2009). Attenuation of Scalar Fluxes Measured with Spatially-displaced Sensors. *Boundary-Layer Meteorology, 130*, 275-300

Huang, Y., Ryu, Y., Jiang, C., Kimm, H., Kim, S., Kang, M., & Shim, K. (2018). BESS-Rice: A remote sensing derived and biophysical process-based rice productivity simulation model. *Agricultural and Forest Meteorology, 256*, 253-269

Jacquemoud, S., & Baret, F. (1990). PROSPECT: A model of leaf optical properties spectra. *Remote Sensing of Environment, 34*, 75-91

Jacquemoud, S., Verhoef, W., Baret, F., Bacour, C., Zarco-Tejada, P.J., Asner, G.P., Fran ̧ois, C., & Ustin, S.L. (2009). PROSPECT+ SAIL models: A review of use for vegetation characterization. *Remote Sensing of Environment, 113*, S56-S66

Jenkins, J.P., Richardson, A.D., Braswell, B.H., Ollinger, S.V., Hollinger, D.Y., & Smith, M.L. (2007). Refining light-use efficiency calculations for a deciduous forest canopy using simultaneous tower-based carbon flux and radiometric measurements. *Agricultural and Forest Meteorology, 143*, 64-79

Jiang, C., & Ryu, Y. (2016). Multi-scale evaluation of global gross primary productivity and evapotranspiration products derived from Breathing Earth System Simulator (BESS). *Remote Sensing of Environment, 186*, 528-547

Joiner, J., Yoshida, Y., Vasilkov, A., Schaefer, K., Jung, M., Guanter, L., Zhang, Y., Garrity, S., Middleton, E.M., Huemmrich, K.F., Gu, L., & Marchesini, L.B. (2014). The seasonal cycle of satellite chlorophyll fluorescence observations and its relationship to vegetation phenology and ecosystem atmosphere carbon exchange. *Remote Sensing of Environment, 152*, 375-391

Kang, M., Malla Thakuri, B., Kim, J., Chun, J., & Cho, C. (2016). A modification of the moving point test method for nighttime eddy flux filtering on hilly and complex terrain. In, *AGU Fall Meeting Abstracts*

Kang, M., Ruddell, B.L., Cho, C., Chun, J., & Kim, J. (2017). Identifying CO2 advection on a hill slope using information flow. *Agricultural and Forest Meteorology, 232*, 265-278

Kljun, N., Calanca, P., Rotach, M., & Schmid, H. (2015). A simple two-dimensional parameterisation for Flux Footprint Prediction (FFP). *Geoscientific Model Development, 8*, 3695

Knohl, A., & Baldocchi, D.D. (2008). Effects of diffuse radiation on canopy gas exchange processes in a forest ecosystem. *Journal of Geophysical Research-Biogeosciences, 113*, doi:10.1029/2007JG000663

Knorr, W. (2000). Annual and interannual CO2 exchanges of the terrestrial biosphere: process-based simulations and uncertainties. *Global Ecology and Biogeography, 9*, 225-252

Kumar, D. (2008). *Definitional glossary of agricultural terms*. IK International Pvt Ltd

Liu, L., Liu, X., Wang, Z., & Zhang, B. (2016). Measurement and analysis of bidirectional SIF emissions in wheat canopies. *IEEE Transactions on Geoscience and Remote Sensing, 54*, 2640-2651

Liu, L.Y., Guan, L.L., & Liu, X.J. (2017). Directly estimating diurnal changes in GPP for C3 and C4 crops using far-red sun-induced chlorophyll fluorescence. *Agricultural and Forest Meteorology, 232*, 1-9

Lloyd, J., & Taylor, J. (1994). On the temperature dependence of soil respiration. *Functional ecology, 8*, 315-323

Lu, C.M., Lu, Q.T., Zhang, J.H., & Kuang, T.Y. (2001). Characterization of photosynthetic pigment composition, photosystem II photochemistry and thermal energy dissipation during leaf senescence of wheat plants grown in the field. *Journal of Experimental Botany, 52*, 1805-1810

Maclean, J., Hardy, B., & Hettel, G. (2013). *Rice Almanac: Source book for one of the most important economic activities on earth*. IRRI

Mauder, M., & Foken, T. (2011). Documentation and instruction manual of the eddy-covariance software package TK3

Mcmillen, R.T. (1988). An Eddy-Correlation Technique with Extended Applicability to Non-Simple Terrain. *Boundary-Layer Meteorology, 43*, 231-245

Meroni, M., Rossini, M., Guanter, L., Alonso, L., Rascher, U., Colombo, R., & Moreno, J. (2009). Remote sensing of solar-induced chlorophyll fluorescence: Review of methods and applications. *Remote Sensing of Environment, 113*, 2037-2051

Miao, G.F., Guan, K.Y., Yang, X., Bernacchi, C.J., Berry, J.A., DeLucia, E.H., Wu, J., Moore, C.E., Meacham, K., Cai, Y.P., Peng, B., Kimm, H., & Masters, M.D. (2018). Sun-Induced Chlorophyll Fluorescence, Photosynthesis, and Light Use Efficiency of a Soybean Field from Seasonally Continuous Measurements. *Journal of Geophysical Research-Biogeosciences, 123*, 610-623

Michalsky, J.J., Berndt, J.L., & Schuster, G.J. (1986). A microprocessor-based rotating shadowband radiometer. *Solar Energy, 36*, 465-470

Michalsky, J.J., Perez, R., Stewart, R., Lebaron, B.A., & Harrison, L. (1988). Design and development of a rotating shadowband radiometer solar radiation/daylight network. *Solar Energy, 41*, 577-581

Monteith, J.L. (1972). Solar Radiation and Productivity in Tropical Ecosystems. *Journal of Applied Ecology, 9*, 747-766

Myneni, R.B., Hoffman, S., Knyazikhin, Y., Privette, J.L., Glassy, J., Tian, Y., Wang, Y., Song, X., Zhang, Y., & Smith, G.R. (2002). Global products of vegetation leaf area and fraction absorbed PAR from year one of MODIS data. *Remote Sensing of Environment, 83*, 214-231

Papale, D., Reichstein, M., Aubinet, M., Canfora, E., Bernhofer, C., Kutsch, W., Longdoz, B., Rambal, S., Valentini, R., Vesala, T., & Yakir, D. (2006). Towards a standardized processing of Net Ecosystem Exchange measured with eddy covariance technique: algorithms and uncertainty estimation. *Biogeosciences, 3*, 571-583

Pinto, F., Müller-Linow, M., Schickling, A., Cendrero-Mateo, M.P., Ballvora, A., & Rascher, U. (2017). Multiangular observation of canopy sun-induced chlorophyll fluorescence by combining imaging spectroscopy and stereoscopy. *Remote Sensing, 9*, 415

Porcar-Castell, A., Tyystjarvi, E., Atherton, J., van der Tol, C., Flexas, J., Pfundel, E.E., Moreno, J., Frankenberg, C., & Berry, J.A. (2014). Linking chlorophyll a fluorescence to photosynthesis for remote sensing applications: mechanisms and challenges. *Journal of Experimental Botany, 65*, 4065-4095

Reichstein, M., Falge, E., Baldocchi, D., Papale, D., Aubinet, M., Berbigier, P., Bernhofer, C., Buchmann, N., Gilmanov, T., Granier, A., Grunwald, T., Havrankova, K., Ilvesniemi, H., Janous, D., Knohl, A., Laurila, T., Lohila, A., Loustau, D., Matteucci, G., Meyers, T., Miglietta, F., Ourcival, J.M., Pumpanen, J., Rambal, S., Rotenberg, E., Sanz, M., Tenhunen, J., Seufert, G., Vaccari, F., Vesala, T., Yakir, D., & Valentini, R. (2005). On the separation of net ecosystem exchange into assimilation and ecosystem respiration: review and improved algorithm. *Global Change Biology, 11*, 1424-1439

Rossini, M., Meroni, M., Migliavacca, M., Manca, G., Cogliati, S., Busetto, L., Picchi, V., Cescatti, A., Seufert, G., & Colombo, R. (2010). High resolution field spectroscopy measurements for estimating gross ecosystem production in a rice field. *Agricultural and Forest Meteorology, 150*, 1283-1296

Ruimy, A., Jarvis, P., Baldocchi, D., & Saugier, B. (1995). CO 2 fluxes over plant canopies and solar radiation: a review. *Advances in ecological research, 26*, 1-68

Running, S.W., Nemani, R.R., Heinsch, F.A., Zhao, M.S., Reeves, M., & Hashimoto, H. (2004). A continuous satellite-derived measure of global terrestrial primary production. *Bioscience, 54*, 547-560

Ryu, Y., Baldocchi, D.D., Kobayashi, H., Ingen, C., Li, J., Black, T.A., Beringer, J., Gorsel, E., Knohl, A., & Law, B.E. (2011). Integration of MODIS land and atmosphere products with a coupled-process model to estimate gross primary productivity and evapotranspiration from 1 km to global scales. *Global Biogeochemical Cycles, 25(GB4017)*, http://dx.doi.org/10.1029/2011GB004053

Ryu, Y., Baldocchi, D.D., Verfaillie, J., Ma, S., Falk, M., Ruiz-Mercado, I., Hehn, T., & Sonnentag, O. (2010a). Testing the performance of a novel spectral reflectance sensor, built with light emitting diodes (LEDs), to monitor ecosystem metabolism, structure and function. *Agricultural and Forest Meteorology, 150*, 1597-1606

Ryu, Y., Jiang, C., Kobayashi, H., & Detto, M. (2018). MODIS-derived global land products of shortwave radiation and diffuse and total photosynthetically active radiation at 5 km resolution from 2000. *Remote Sensing of Environment, 204*, 812-825

Ryu, Y., Kang, S., Moon, S.K., & Kim, J. (2008). Evaluation of land surface radiation balance derived from Moderate Resolution Imaging Spectrometer (MODIS) over complex terrain and heterogeneous landscape on clear sky days. *Agricultural and Forest Meteorology, 148*, 1538-1552

Ryu, Y., Lee, G., Jeon, S., Song, Y., & Kimm, H. (2014). Monitoring multi-layer canopy spring phenology of temperate deciduous and evergreen forests using low-cost spectral sensors. *Remote Sensing of Environment, 149*, 227-238

Ryu, Y., Sonnentag, O., Nilson, T., Vargas, R., Kobayashi, H., Wenk, R., & Baldocchi, D.D. (2010b). How to quantify tree leaf area index in an open savanna ecosystem: A

multi-instrument and multi-model approach. *Agricultural and Forest Meteorology, 150*, 63-76

Sato, H., Kumagai, T.o., Takahashi, A., & Katul, G.G. (2015). Effects of different representations of stomatal conductance response to humidity across the African continent under warmer CO2-enriched climate conditions. *Journal of Geophysical Research: Biogeosciences, 120*, 979-988

Sellers, P.J. (1985). Canopy Reflectance, Photosynthesis and Transpiration. *International Journal of Remote Sensing, 6*, 1335-1372

van der Tol, C., Berry, J.A., Campbell, P.K., & Rascher, U. (2014). Models of fluorescence and photosynthesis for interpreting measurements of solar-induced chlorophyll fluorescence. *Journal of Geophysical Research: Biogeosciences, 119*, 2312-2327

van der Tol, C., Rossini, M., Cogliati, S., Verhoef, W., Colombo, R., Rascher, U., & Mohammed, G. (2016). A model and measurement comparison of diurnal cycles of sun-induced chlorophyll fluorescence of crops. *Remote Sensing of Environment, 186*, 663-677

van der Tol, C., Verhoef, W., Timmermans, J., Verhoef, A., & Su, Z. (2009). An integrated model of soil-canopy spectral radiances, photosynthesis, fluorescence, temperature and energy balance. *Biogeosciences, 6*, 3109-3129

Van Dijk, A., Moene, A., & De Bruin, H. (2004). The principles of surface flux physics: theory, practice and description of the ECPACK library. *Internal Rep, 1*, 99

Verhoef, W. (1984). Light scattering by leaf layers with application to canopy reflectance modeling: The SAIL model. *Remote Sensing of Environment, 16*, 125-141

Verma, M., Schimel, D., Evans, B., Frankenberg, C., Beringer, J., Drewry, D.T., Magney, T., Marang, I., Hutley, L., Moore, C., & Eldering, A. (2017). Effect of environmental conditions on the relationship between solar-induced fluorescence and gross primary productivity at an OzFlux grassland site. *Journal of Geophysical Research: Biogeosciences, 122*, 716-733

Von Caemmerer, S. (2000). *Biochemical models of leaf photosynthesis*. Csiro publishing

Wagle, P., Zhang, Y., Jin, C., & Xiao, X. (2016). Comparison of solar-induced chlorophyll fluorescence, light-use efficiency, and process-based GPP models in maize. *Ecol Appl, 26*, 1211-1222

Wingler, A., Mares, M., & Pourtau, N. (2004). Spatial patterns and metabolic regulation of photosynthetic parameters during leaf senescence. *New Phytologist, 161*, 781-789

Wit, C.T.d. (1965). Photosynthesis of leaf canopies. In, *Agricultural research reports, 663*. Wageningen: Pudoc

Yang, H., Yang, X., Zhang, Y., Heskel, M.A., Lu, X., Munger, J.W., Sun, S., & Tang, J. (2017). Chlorophyll fluorescence tracks seasonal variations of photosynthesis from leaf to canopy in a temperate forest. *Global Change Biology, 23*, 2874-2886

Yang, P., & van der Tol, C. (2018). Linking canopy scattering of far-red sun-induced chlorophyll fluorescence with reflectance. *Remote Sensing of Environment, 209*, 456-467

Yang, X., Tang, J., Mustard, J.F., Lee, J.E., Rossini, M., Joiner, J., Munger, J.W., Kornfeld, A., & Richardson, A.D. (2015). Solar-induced chlorophyll fluorescence that correlates with canopy photosynthesis on diurnal and seasonal scales in a temperate deciduous forest. *Geophysical Research Letters, 42*, 2977-2987

Zarco-Tejada, P.J., Catalina, A., González, M.R., & Martín, P. (2013a). Relationships between net photosynthesis and steady-state chlorophyll fluorescence retrieved from airborne hyperspectral imagery. *Remote Sensing of Environment, 136*, 247-258

Zarco-Tejada, P.J., González-Dugo, M.V., & Fereres, E. (2016). Seasonal stability of chlorophyll fluorescence quantified from airborne hyperspectral imagery as an indicator of net photosynthesis in the context of precision agriculture. *Remote Sensing of Environment, 179*, 89-103

Zarco-Tejada, P.J., Morales, A., Testi, L., & Villalobos, F.J. (2013b). Spatio-temporal patterns of chlorophyll fluorescence and physiological and structural indices acquired from hyperspectral imagery as compared with carbon fluxes measured with eddy covariance. *Remote Sensing of Environment, 133*, 102-115

Zhang, Y., Guanter, L., Berry, J.A., Joiner, J., van der Tol, C., Huete, A., Gitelson, A., Voigt, M., & Kohler, P. (2014). Estimation of vegetation photosynthetic capacity from space-based measurements of chlorophyll fluorescence for terrestrial biosphere models. *Globle Change Biology, 20*, 3727-3742

Zhang, Y., Xiao, X.M., Jin, C., Dong, J.W., Zhou, S., Wagle, P., Joiner, J., Guanter, L., Zhang, Y.G., Zhang, G.L., Qin, Y.W., Wang, J., & Moore, B. (2016a). Consistency between sun-induced chlorophyll fluorescence and gross primary production of vegetation in North America. *Remote Sensing of Environment, 183*, 154-169

Zhang, Y.G., Guanter, L., Berry, J.A., van der Tol, C., Yang, X., Tang, J.W., & Zhang, F.M. (2016b). Model-based analysis of the relationship between sun-induced chlorophyll fluorescence and gross primary production for remote sensing applications. *Remote Sensing of Environment, 187*, 145-155

Zoogman, P., Liu, X., Suleiman, R.M., Pennington, W.F., Flittner, D.E., Al-Saadi, J.A., Hilton, B.B., Nicks, D.K., Newchurch, M.J., Carr, J.L., Janz, S.J., Andraschko, M.R.,

Arola, A., Baker, B.D., Canova, B.P., Miller, C.C., Cohen, R.C., Davis, J.E., Dussault, M.E., Edwards, D.P., Fishman, J., Ghulam, A., Abad, G.G., Grutter, M., Herman, J.R., Houck, J., Jacob, D.J., Joiner, J., Kerridge, B.J., Kim, J., Krotkov, N.A., Lamsal, L., Li, C., Lindfors, A., Martin, R.V., McElroy, C.T., McLinden, C., Natraj, V., Neil, D.O., Nowlan, C.R., O'Sullivan, E.J., Palmer, P.I., Pierce, R.B., Pippin, M.R., Saiz-Lopez, A., Spurr, R.J.D., Szykman, J.J., Torres, O., Veefkind, J.P., Veihelmann, B., Wang, H., Wang, J., & Chance, K. (2017). Tropospheric emissions: Monitoring of pollution (TEMPO). *Journal of Quantitative Spectroscopy & Radiative Transfer, 186*, 17-39

Zou, X., & Mõttus, M. (2015). Retrieving crop leaf tilt angle from imaging spectroscopy data. *Agricultural and Forest Meteorology, 205*, 73-82

Supplementary Materials

A. SiF Retrieval Method

In this study, SiF values were retrieved in the range of 745 to 780 nm using the singular vector decomposition method (SVD) (Guanter et al. 2012; Guanter et al. 2013). In SVD, upwelling irradiance can be expressed as

$$I_{out} = I_{in} \sum_{i=0}^{n} a_i \lambda^i + h_F Fs \quad \text{(S1)}$$

Where I_{out} corresponds to upwelling irradiance; I_{in} represents downwelling irradiance above the canopy; λ is the vector of measured wavelengths; h_F is a fixed vector which accounts for the spectral shape of fluorescence; and Fs is a scalar representing magnitude of fluorescence at a predetermined wavelength. The polynomial in λ describes the low spectral frequency contribution because of vegetation reflectance. SiF values are calculated by solving Equation S1 for Fs using linear regression. With the ground-based measurements, I_{out} and I_{in} are known, and h_F is generated from leaf level measurement from Global Ecology Lab at Carnegie Institution of Washington. Then the retrieval state vector consists of the polynomial coefficients a_i and Fs.

I_{in} is reconstructed using several spectral vectors derived by SVD method from a training set without contribution of fluorescence. To model the vegetation reflectance, the first and second singular vectors carrying most of the spectrum

information are convolved with a polynomial accounting for low frequency changes in the continuum. The resulting forward model can be written as

$$I_{out} = v_1 \sum_{i=1}^{n} a_i \lambda^i + v_2 \sum_{i=1}^{n} b_i \lambda^i + \sum_{i=1}^{n_v} c_i \, v_i + h_F Fs \qquad \text{(S2)}$$

where v_i are singular vectors derived from training set; n is the degree of the polynomial; and n_v is the number of singular vectors used to reconstruct incoming irradiance (Guanter et al. 2012). The Equation S2 can be solved by means of standard least squares fitting.

In this paper, we derived all parameters in Equation S2 from our ground measurements. The training dataset (Figure S1) included downwelling irradiance spectrum from uplooking probe, and upwelling irradiance spectrum from downlooking probe when there was no rice planted, including bare soil, water and snow signals. We used the same training dataset for the whole growing season that included all relevant variations (diurnal and seasonal variations of solar spectrum, and spectra shift of fiber optics with time). In particular, the spectra before the rice transplanting were found to be necessary to account for the spectral differences between up- and downward pointing fiber readings. We analyzed the influence of singular vectors number on retrieving SiF, and found that the relative RMSE of reconstructed spectrum decreased with singular vector numbers and SiF retrievals stabilized when singular vectors were around 300. We then extracted the top 300 singular vectors to reconstruct the spectrum without fluorescence contribution. Consistent with Guanter et al. (2013), we also found that for a broad spectral fitting window (745-780 nm), cubic polynomial performed better than quadratic polynomial function to represent low spectral frequency changes in the continuum due to surface reflectance. We therefore set the degree of both polynomial functions as cubic.

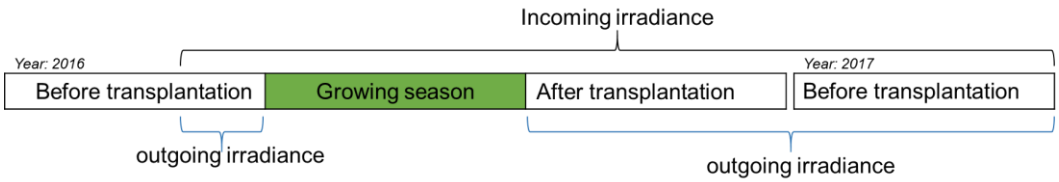

Figure S1. Training dataset composition used in the SVD SiF retrieval. In total, around 210 days for incoming irradiance and around 180 days for outgoing irradiance were included.

Furthermore, we evaluated the SiF retrieval method on simulated upwelling irradiance spectra with known reflectance and known fluorescence magnitudes. The simulated upwelling irradiance was calculated as

$$I_{out}^{sim} = I_{in}^{mea} \times ref_{sim} + SiF_{sim} \quad \text{(S3)}$$

where I_{in}^{mea} is measured downwelling irradiance from uplooking probe; ref_{sim} is simulated canopy reflectance using the PROSAIL model; and SiF_{sim} represents canopy fluorescence with known magnitude and fixed spectral shape. We used two sets of simulated upwelling irradiance with different temporal variations to calculate SiF. In the first simulation, SiF has an apparent seasonal variation but no diurnal variation, and its values range continuously from 0 to around 7 $mWm^{-2}s^{-1}$. In the second simulation, SiF has a consistent diurnal variation over the whole growing season, and its value changes discretely from 0 to around 10 $mWm^{-2}s^{-1}$. Derived SiF values were compared with the true magnitude (Figure S2).

The calculation method was demonstrated to be able to retrieve canopy SiF. To ensure data quality, retrieved SiF values whose rRMSE of reconstructed irradiance spectrum was larger than 0.15% or whose relative error of retrieved SiF was larger than 25% were excluded (Figure S2 a, b, c, d). From simulation one, we found that computed SiF well tracked the seasonal variations of true SiF values, and they showed a strong 1:1 linear relationship (R2 = 0.97, Figure S2e). For simulation two, retrieved SiF also presented the same diurnal courses with its true

values (R2 = 0.94, Figure S2f). Although given the same true SiF value, computed SiF showed a considerable variation, the mean of computed SiF was always around 90% of its true value and the standard deviations were consistent over different SiF values (around 5%). Therefore, we were confident that the random variation had no significant influence on the seasonal or diurnal patterns of canopy SiF (SiF values were reported at 760 nm).

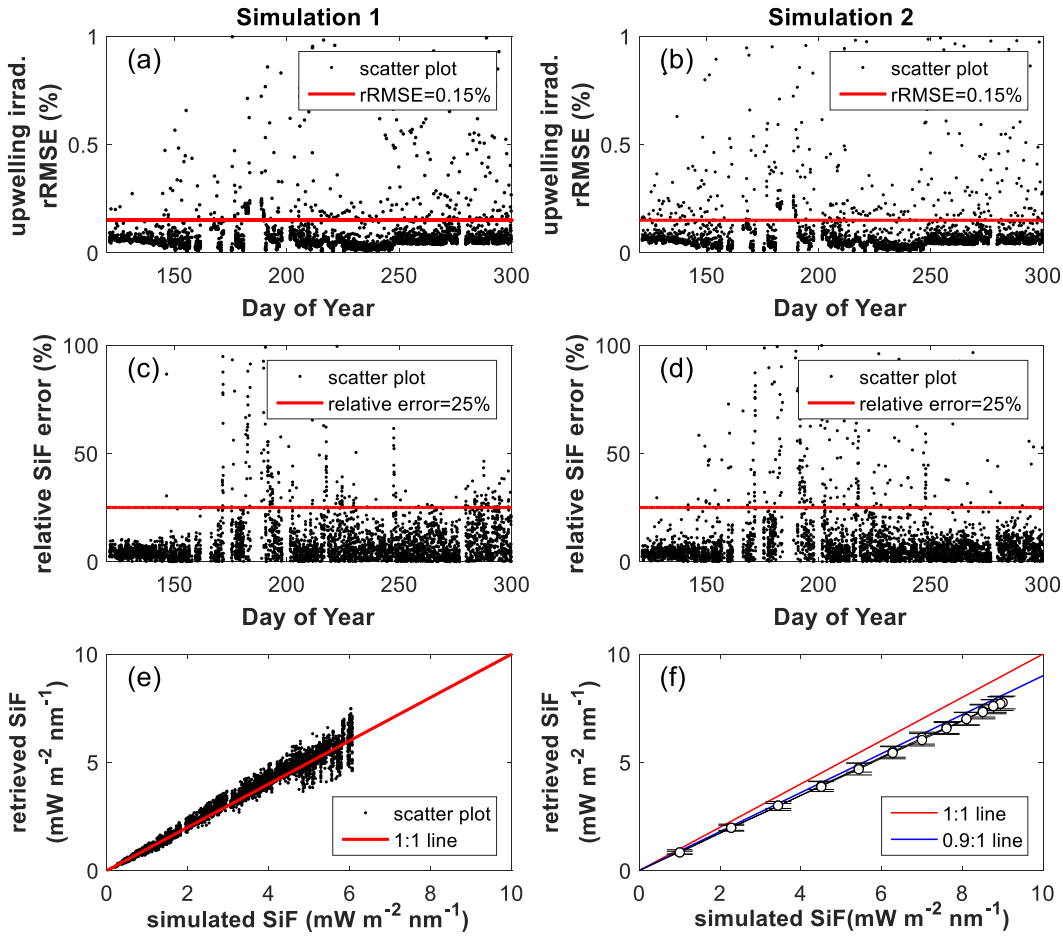

Figure S2. Temporal variations of relative RMSE (RMSE / mean) between simulated (from Equation S3) and reconstructed upwelling irradiance using SVD method (from Equation S2) (a, b). Relative error ($\sqrt{(y_{sim,reference} - y_{sim,retrieved})^2}/y_{sim,reference}$) between the reference values of the SiF simulation (from Equation S3) and SiF retrieval using SVD method

(from Equation S2) (c, d).Comparison between simulated and retrieved SiFs, and only filtered values are shown (e, f). Error bars in (f) represent standard deviation.

B. Temporal Variations of Environmental Measurements

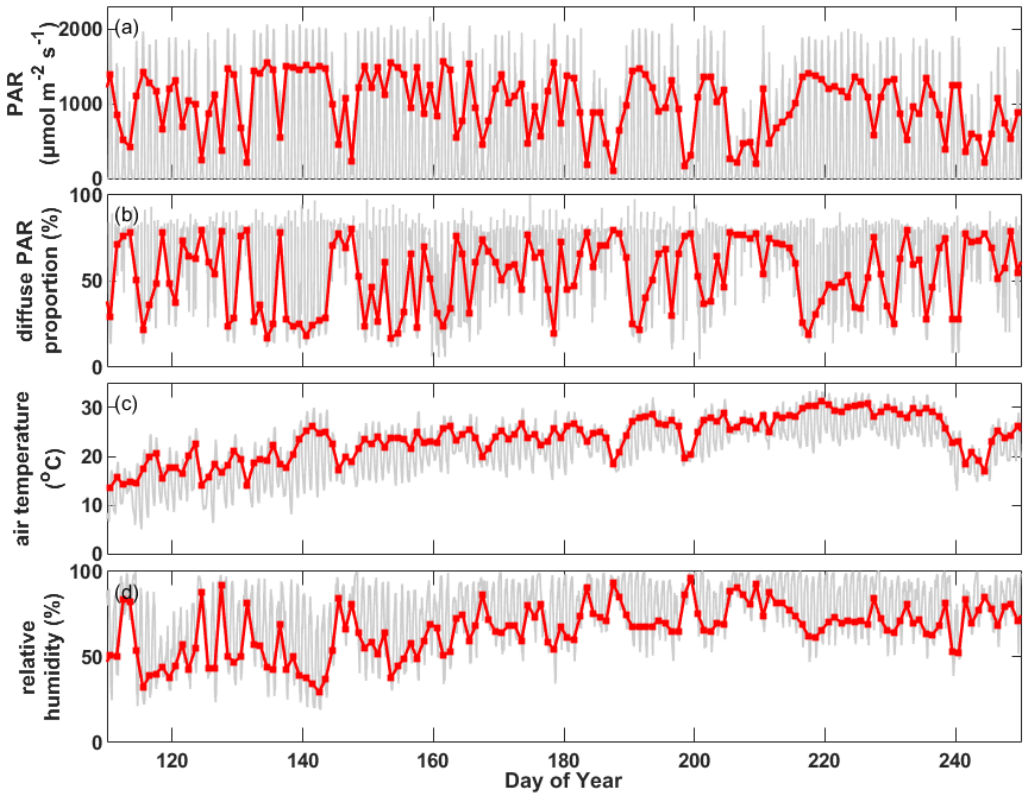

Figure S3. Temporal variations of (a) photosynthetically active radiation (PAR); (b) diffuse PAR proportion; (c) air temperature and (d) relative humidity in 2016. Light gray line represents half hourly measurements. Red line represents daily mean of half hourly measurements from 08:00 to 18:00 local time.

C. Simulation of Absorbed PAR

The diurnal patterns of measured absorbed PAR were adjusted and data gaps were filled with PROSAIL simulations. Since LED sensors used to measure

transmitted PAR were located between rice rows, the diurnal absorbed PAR had a clear tendency to be underestimated, especially at noon. Input parameters for PROSAIL model had three sources. The first one was field measurements in 2016. The second one was field measurements in 2017. Since the general growing environments were quite similar in 2016 and 2017, field measurements in 2017 was also used to simulate absorbed PAR in 2016. The final one was the LOPEX93 database (http://opticleaf.ipgp.fr). Input parameters were shown in the following table (Table S1).

Table S1. Input parameters for PROSAIL model.

Parameter	Source	Value
Chlorophyll ab content	Field measurement in 2017	
Carotenoid content	Field measurement in 2017	25% of chlorophyll ab content
Brown pigment content	Field measurement in 2016	Yellow leaf fraction
Leaf water equivalent layer	LOPEX93 database	0.0104 cm
Dry matter content	Field measurement in 2016	
Leaf thickness parameters	LOPEX93 database	1.7544
Leaf area index	Field measurement in 2016	
Leaf inclination angle	Field measurement in 2017	

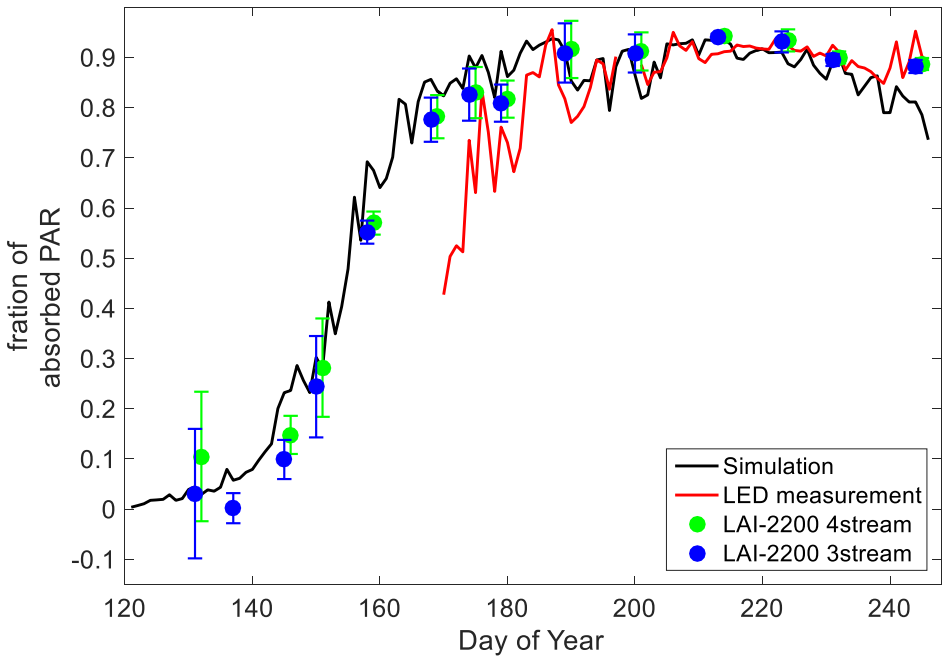

Figure S4. Seasonal variations of fraction of absorbed PAR from PROSAL simulation, LED sensors measurement and manual measurement of LAI-2200. Error bars represent standard deviation.

Seasonal variations of measurements from LAI-2200 and PROSAIL simulations agreed well with each other (Figure S4). A clear underestimation from LED measurements could be observed from around DOY 170 to 190. The R^2 of linear regression between automatically measured and simulated APAR ranged from 0.18 to 0.91 on individual dates, with a mean value of 0.56 over the whole growing season. Diurnal APAR measurements were modified with linear regressions between measurements and simulations on individual days.

D. Influence of Air Temperature and Relative Humidity on Relationship Between SiF and GPP

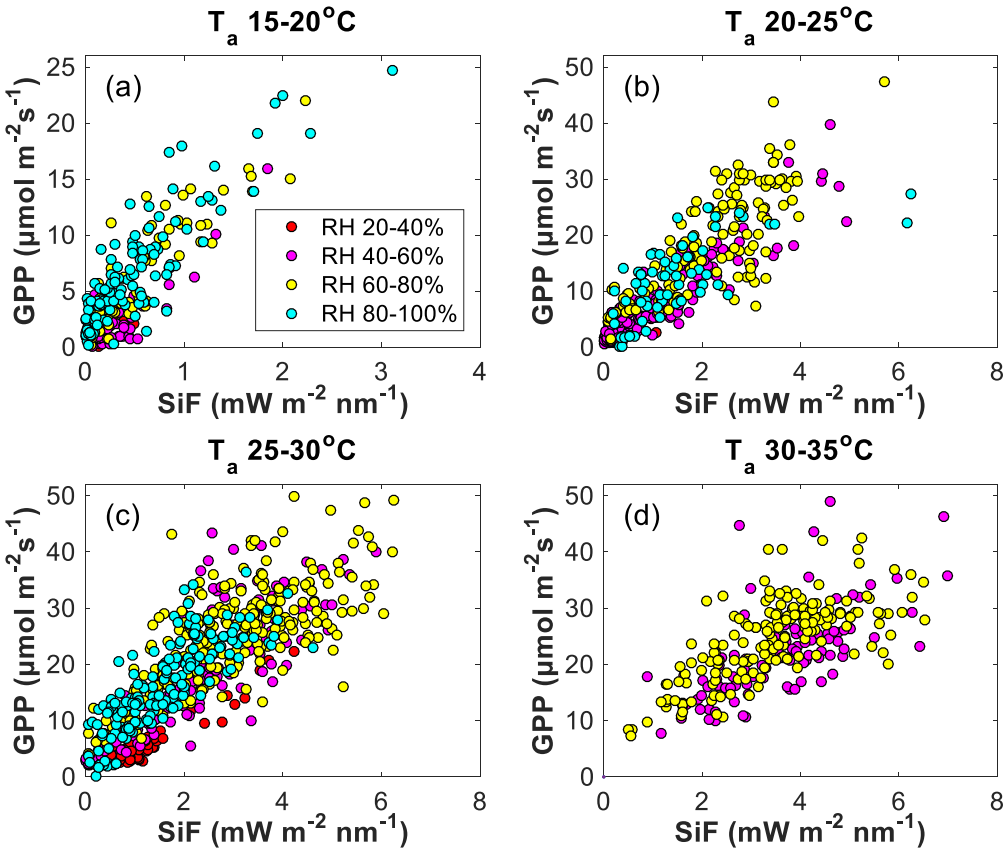

Figure S5. Scatter plot of half hourly SiF and GPP given different ranges of air temperature (T_a) and relative humidity (RH) over the whole growing season.

Table S2. Coefficients of determination of fitted linear regressions ($y = a \times x$) between half hourly SiF and GPP over different air temperature and relative humidity values. '/' indicates absence of data corresponding to certain range of air temperature and relative humidity. *p*-values are less than 0.05 except for '*' ($p > 0.05$).

Air temperature (℃)	Relative humidity (%)			
	20-40	40-60	60-80	80-100
15-20	*	0.67	0.73	0.67
20-25	-0.78	0.83	0.61	0.40
25-30	0.77	0.67	0.35	0.52

30-35	/	0.36	0.21	/

국문 초록

태양 유도 엽록소 형광 (SiF)은 총 일차 생산량 (GPP)의 직접적인 지표로 최근들어 각광받고 있다. 지상 관측, 항공기 및 위성 관측 연구에 따르면 계절규모에서 SiF 와 GPP 사이의 강한 선형 관계를 보여 주지만, 일별에서 계절적 규모에 걸친 고해상도 시간 해상도에서의 관계는 분명하지 않다. 이 연구에서, 벼논 군락 SiF, GPP 및 흡수 된 광합성 유효복사 (APAR)을 철원 농경지에서 2016 년 전체 생장 기간 동안 자동화 된 스펙트럼 시스템 및 에디 플럭스 타워를 사용하여 지속적으로 모니터링하였다. 30 분 단위로 볼때, 전체 성장기간 동안 SiF 와 GPP (R^2 = 0.76) 및 APAR 과 GPP (R^2 = 0.76) 간의 강한 선형 관계가 관찰되었다. 상대 습도, 산란 PAR 비율 그리고 벼 생장단계가 SiF 와 GPP, APAR 및 GPP 사이의 관계에 영향을 미치는 것을 발견하였다. 이 요인들을 다중 회귀 분석에 반영했을때 R^2 = 0.83 (SiF:GPP) 및 R^2 = 0.88 (APAR:GPP) 까지 각각 향상된다는 것을 발견했다. LUE_p (= GPP / APAR)와 LUE_f (= SiF / APAR) 사이의 관계는 30 분 해상도에서는 나타나지 않았고 일평균 해상도에서도 약하게 나타났다 (R^2 = 0.24). 30 분 단위로 분석할때 SiF 와 GPP 또는 APAR 과 GPP 보다 SiF 와 APAR 간의 선형 관계가 훨씬 강하다는 사실을 발견했다. 전반적으로, 우리의 결과는 시간 해상도와 시간 규모에 관계없이 논 군락의 SiF 는 APAR 를 반영하였으며, 따라서 SiF 를

이용하여 GPP 를 추정하기 위해서는 LUE_p 를 모델링해야함을 나타냈다. 이러한 결과는 여러 시간 규모에서 군락 SiF 와 GPP 간의 관계를 기작에 기반하여 이해하는데 기여할 것이다.

Acknowledgement

First, I would first like to thank my supervisor, Dr. Youngryel Ryu of the Interdisciplinary Program in Agricultural and Forest Meteorology at Seoul National University. The door to Prof. Ryu's office was always open whenever I ran into a trouble spot of my research or writing. He helped me to develop many professional skills that are useful for both current and future studies.

In addition, I really appreciate the two experts who were involved in the evaluation for this thesis: Dr. Hyunseok Kim and Dr. Kwangsoo Kim. Without their passionate participation and insightful comments, the thesis could not have been successfully conducted.

I would also like to acknowledge Dr. Benjamin Dechant as the second reader of my research results, and I am gratefully indebted to his very valuable comments on this study. I also want to thank all my current and previous lab members, Yorum Hwang, Dr. Chongya Jiang, Jongmin Kim, Hyungsuk Kimm, Soyoun Kim, Dr. Yan Huang, Juwon Kong and Ms. Yunah Lee for tedious field works, constructive discussions and countless kindness during the past two years.

Finally, I must express my very profound gratitude to my mother for providing me with unfailing support and continuous encouragement throughout my years of study. This accomplishment would not have been possible without any of them. Thank you very much!

This research was funded by the National Research Foundation of Korea (NRF-2016M1A3A3A02018195) and the Korea Meteorological Administration Research and Development Program under the Grant Weather Information Service Engine (WISE) project (KMA-2012-0001-A). We thank Dennis Baldocchi and

Joseph Verfaillie at UC Berkeley who kindly shared technical details in their diffuse PAR sensor, and Minkyu Moon who made the diffuse PAR sensor.

The contents of this thesis will appear in the following peer review paper which was proof stage when this thesis was submitted: Yang, K., Ryu, Y.*, Dechant, B., Berry, J.A., Hwang, Y., Jiang, C., Kang, M., Kim, J., Kimm, H., Kornfeld, A., & Yang, X. (2018). Sun-induced chlorophyll fluorescence is more strongly related to absorbed light than to photosynthesis at half-hourly resolution in a rice paddy. Remote Sensing of Environment. https://doi.org/10.1016/j.rse.2018.07.008

Author

Kaige Yang